



Gas-particle partitioning of m-xylene and naphthalene oxidation products: temperature and NO_x influence

Marwa Shahin¹, Julien Kammer¹, Brice Temime-Roussel¹, and Barbara D'Anna¹

¹Aix-Marseille Univ., CNRS, LCE, Marseille, France

5 Correspondence to: Barbara D'Anna (barbara.danna@univ-amu.fr), Marwa Shahin (marwa.shahin@etu.univ-amu.fr)

Abstract. Volatile organic compounds (VOCs) react with atmospheric oxidants resulting in oxygenated products of lower volatility known as semi and intermediate volatile organic compounds (S/IVOCs) forming secondary organic aerosols (SOA). Those compounds can partition between the gas and particle phases, a critical process influenced by several environmental parameters, yet poorly constrained. This study aims to evaluate the effect of temperature and VOC/NO_x ratio on SOA formation and partitioning of individual SOA products from m-xylene and naphthalene OH-oxidation. Experiments are carried out in an oxidation flow reactor (OFR) and products are identified and quantified using a proton transfer reaction time-of-flight mass spectrometer (PTR-ToF-MS) coupled to a CHemical Analysis of aeRosol ONline (CHARON) inlet. Results show that lower temperatures significantly enhance SOA formation, while lower VOC/NO_x ratios reduce it. Gas-phase m-xylene major products are C₃, C₅ and C₈ whereas particle-product distributions exhibit a progressive increase from C₂ to C₈. In contrast, naphthalene products partition more readily into the condensed phase, with C₈-C₁₀ products dominating. Most of the oxidation products from both precursors exhibit a volatility distribution in the SVOC regime, with fewer in the IVOC regime. The decrease in temperature shifts saturation concentration (C_i^*) values towards lower values, though no clear relationship between C_i^* and oxidation state is observed. A comparison between observed and estimated volatilities using SIMPOL.1 model reveals systematic deviations for both light molecules and heavy compounds, suggesting a need for improved predictive models.

20 1 Introduction

Aromatic hydrocarbons (AHs) are an ubiquitous class of air pollutants and contribute to an important fraction of the total volatile organic compounds (VOCs) in urban environments; the relative contribution may vary and depends on location and season (Calvert et al., 2002; Jiang et al., 2017; Montero-Montoya et al., 2018). Among the different AHs, xylene and naphthalene are important anthropogenic VOCs primarily emitted from petrochemical industries, biomass burning, diesel and gasoline engines, or through solvent evaporation (Fang et al., 2021, 2024; Wu et al., 2020; Xuan et al., 2021). In the atmosphere, AHs react with common oxidants as hydroxyl (OH), nitrate (NO₃) and chloride (Cl) radicals and ozone (O₃) leading to the formation of oxygenated reaction products of lower vapor pressures also known as semi-volatile organic compounds (SVOCs) and intermediate-volatile organic compounds (IVOCs) (Seinfeld and Pandis, 2016). These compounds may partition to the particle phase forming secondary organic aerosols (SOA) that represent approximately 60% of ambient



30 organic aerosol (Huang et al., 2020, 2014) and have an impact on visibility (Li et al., 2014; Liu et al., 2017), climate (Liu and Matsui, 2020; Shrivastava et al., 2017) and human health (Anderson et al., 2012; Berlinger et al., 2024; Singh and Tripathi, 2021; Thangavel et al., 2022). Indeed, particulate air pollution is closely correlated to the progression of numerous respiratory diseases, in addition to cancer, cardiovascular diseases, and neurological damage (Liu et al., 2022a; Singh and Tripathi, 2021; Song et al., 2017; Thangavel et al., 2022). In the EU, each year, around 238,000 premature deaths are attributable to fine
35 particulate matter (PM_{2.5}) exposure (European Environment Agency, 2022). Improving our understanding of particle sources and properties is thus pivotal to improve a more sustainable environment.

Over the last decades, many laboratory and modelling studies investigated SOA generated by AHs reaction products (Chen et al., 2018; Forstner et al., 1997; Klodt et al., 2023; Lannuque et al., 2018; Li et al., 2022; Liu et al., 2023, 2022b; Lu et al., 2024; Song et al., 2007; Srivastava et al., 2022; Tian et al., 2023). The OH oxidation of monoaromatic compounds operates through
40 two main common pathways (Atkinson et al., 1991; Bloss et al., 2005; Calvert et al., 2002; Forstner et al., 1997; Pan and Wang, 2014). In the case of m-xylene, the first pathway is the OH addition to the aromatic ring, predominantly on the ortho position (Fan and Zhang, 2008) to form a hydroxy-methyl-benzyl radical with a subsequent addition of O₂ to form a bicyclic radical, a major ring opening product channel (Zhao et al., 2005). The second reaction pathway is the H-abstraction from the methyl group to form a methyl benzyl radical, with a subsequent addition of O₂ to form a benzyl peroxy radical (Atkinson et al., 1991;
45 Molina et al., 1999). In the presence of NO_x, the peroxy radical mainly reacts with NO to form an alkoxy radical, and finally an abstraction by O₂ leads to the formation of m-tolualdehyde (Srivastava et al., 2023). In the case of PAHs, such as naphthalene, OH reaction is initiated exclusively by OH addition, most predominantly at the C₁ position (68 %) of the benzene ring (Wang et al., 2007). Then, a hydroxy cyclohexadienyl radical is formed, which further reacts with NO₂ to form nitrogen-containing compounds, or with O₂ to form various products out of which 2-formylcinnamaldehyde is major (Nishino et al.,
50 2009).

A key process determining the fate of the oxidation products generated from AH oxidation is their ability to partition between gas and particle phases, either throughout nucleation forming new particles or by condensing on pre-existing particles. Partitioning is influenced by many environmental parameters such as temperature, relative humidity, the nature and the diameter of the pre-existing particles on which they condense and the physio-chemical properties of the S/IVOC condensing
55 (Kamens et al., 2011; Kim et al., 2007; Lannuque et al., 2018; Loza et al., 2012; Ng et al., 2007; Qi et al., 2010; Sato et al., 2007; Takekawa et al., 2003; Warren et al., 2009; Xu et al., 2015). Lannuque et al. (2023) have studied the gas-particle partitioning of toluene in a similar OFR system. Experiments carried at 280 K were characterised by a higher mass loading in the particle phase compared to those at 295 K, as well as a shift in volatility values of oxidation products towards lower log₁₀C_i^{*} values. The NO_x level has been shown to have significant yet possibly contrasting effects on SOA formation (Chan et al., 2009;
60 Ng et al., 2007; Qi et al., 2020; Song et al., 2005; Zhu et al., 2021). Some studies have reported a decrease in SOA yield under high NO_x conditions which can be explained by the termination reactions of NO with the alkoxy radicals (RO₂, HO₂ and HO), limiting the formation of higher oxygenated compounds that condense into the particle phase (Chan et al., 2009; Ng et al., 2007; Song et al., 2005). In other studies, SOA yields increase up to 60% under elevated levels of NO_x due to the formation

of nitro-aromatic compounds such as nitrophenols, nitrocatechols and nitroresols of low volatility (Srivastava et al., 2023; Zhu et al., 2021). As a result, SOA modelling is complex and not yet satisfactorily constrained, resulting in large uncertainties in the model representation of SOA from AHs (Heald et al., 2005; Lu et al., 2024; Volkamer et al., 2006; Xu et al., 2015; Zhang et al., 2021).

Direct measurements of S/IVOCs in real time is a challenge due to their complexity, diversity, and low concentrations. The analytical development of the “CHemical Analysis of aeRosols ONline” (CHARON) inlet coupled with a proton-transfer-reaction-time of flight-mass spectrometry (PTR-ToF-MS) enables alternative online measurements of both gas and particle phases at molecular level (Eichler et al., 2015). It also allows measuring both gas and particle phases with reduced artefacts associated with particle collection and thermal desorption compared to traditional techniques (Peng et al., 2023). Promising applications have been shown in several laboratory and field studies (Lannuque et al., 2023; Müller et al., 2017; Muller et al., 2017; Piel et al., 2021), while its application to gas-particle partitioning investigations is relatively new (Gkatzelis et al., 2018; Lannuque et al., 2023; Peng et al., 2023; Piel et al., 2021).

The aim of the present study is to evaluate gas-particle partitioning of S/IVOCs involved in SOA formation from the photooxidation of AHs in different conditions. For that purpose, the photooxidation of AH compounds was investigated using an online CHARON-PTR-ToF-MS coupled to an oxidation flow reactor. These laboratory experiments aim at 1) identifying the gas and particle phase products of m-xylene and naphthalene at a molecular level; 2) evaluating the partitioning behaviour of individual SOA products; and 3) assessing the effect of atmospheric conditions (temperature variation and NO_x/VOC ratio) on this partitioning. Two compounds, m-xylene and naphthalene, are selected, for the following reasons, i) their ubiquity in urban areas (Fang et al., 2021; Wu et al., 2020; Xuan et al., 2021) ii) their known reactivity with OH radicals that is in the same order of magnitude (Calvert et al., 2015), and iii) their SOA formation potential has been previously demonstrated (Chan et al., 2009; Chen et al., 2016, 2018; Lu et al., 2024; Ng et al., 2007; Song et al., 2007; Srivastava et al., 2022).

2 Methods

2.1 OFR experimental setup

Photooxidation experiments have been conducted in a 19.3 L cylindrical aerosol oxidation flow reactor (OFR, 153 mm internal diameter, 105 cm length) made up of quartz, vertically oriented, and surrounded by 6 UVB lamps (Helios Italquartz) with a continuous emission spectrum in the 280-350 nm range ($\lambda_{\text{max}} = 310$ nm, Fig. 1). An external air conditioning unit is connected to the tube allowing temperature control in the range 280-295 K. The gas phase stream consists of humid air, the selected VOC precursor (m-xylene or naphthalene), nitrogen dioxide (NO₂) and hydrogen peroxide (H₂O₂). For humidification, two glass bottles containing milliQ water are bubbled at 0.2-1 L min⁻¹ by pure N₂ in order to maintain relative humidity (RH) around 50 % (from 35 % to 65 %, among all experiments). A constant concentration of m-xylene is generated by flowing a constant flow of 0.15 L min⁻¹ of N₂ over a permeation tube containing a pure solution (≥ 99 % purity, Sigma Aldrich) placed in an oven



95 and kept at a constant temperature of 308 K. Some solid naphthalene (99% purity, Sigma Aldrich) is kept in an iced water bath while headspace is flown at 0.1 L min⁻¹ by pure N₂ to generate a constant flow of naphthalene in the flow tube. NO₂ is introduced using a cylinder (100 ± 5 ppm in N₂, Linde) and diluted in N₂ using different mass flow controllers to the desired mixing ratios prior to entering the tube (varying from 40 to 340 ppbV), depending on the required VOC/NO_x conditions. A hydrogen peroxide (H₂O₂) solution (50 % in H₂O, stabilised, Sigma Aldrich) is used as a hydroxyl radical (OH) precursor and
 100 is constantly introduced in the OFR by bubbling pure N₂ in the solution at a flow of 0.1-0.2 L min⁻¹. The average oxidant concentration during the experiment is calculated assuming a pseudo first order reaction rate from the VOC precursor decay ($k_{\text{OH}+\text{xylene}} = 2.3 \times 10^{-11} \text{ cm}^3 \text{ molecules}^{-1} \text{ s}^{-1}$, $k_{\text{OH}+\text{naphthalene}} = 2.3 \times 10^{-11} \text{ cm}^3 \text{ molecules}^{-1} \text{ s}^{-1}$ (Calvert et al., 2015), and with the hypothesis that the other reactions with OH are negligible in the first seconds following lamps switching on. The OH radical concentrations range from 2.2 to $5.4 \times 10^7 \text{ molecules cm}^{-3}$ corresponding approximately to 1.3 and 3 days of atmospheric OH-
 105 radical exposure, taking into account a diurnal average hydroxyl radical concentration of $1.5 \times 10^6 \text{ molecules cm}^{-3}$ (Mao et al., 2009). Due to background contaminations, compounds with *m/z* 61 and below, mainly acetaldehyde, acetic acid, formaldehyde and formic acid, are not considered in further analysis. Monodispersed ammonium sulphate (AS) seeds serve as a pre-existing surface and are generated by nebulizing a 10⁻² M AS solution (99.5 % purity, Acros Organics) using a TSI atomizer (model 3076), dried through a silica diffusion drier and then size selected in an Aerodynamic Aerosol Classifier (AAC, Cambustion) to generate monodisperse aerosols with an average diameter of 200 nm. The overall input flow is 2.4 L
 110 min⁻¹ to ensure a residence time in the tube of 8 mins.

2.2 Instrumentation and data analysis

Figure 1 shows the schematic of the experimental set-up, where several online instruments are used to characterise gas and particle phase chemical compositions as well as particle number and size distribution.

115 A commercial Proton Transfer Reaction-Time of Flight-Mass Spectrometer (PTR-ToF-MS 6000X2, Ionicon Analytik GmbH, Innsbruck, Austria) coupled to a “CHemical Analysis of aeRosols ONline” (CHARON) inlet is used to follow online the gas and particle phase chemical composition of the organic fraction. The CHARON inlet has been already described in detail elsewhere (Eichler et al., 2015; Leglise et al., 2019; Müller et al., 2017). Briefly, the sampled air travels through three major sections of the CHARON inlet 1) a gas phase denuder of activated charcoal that strips off gaseous organics; 2) an aerodynamic
 120 lens system (ADL) that collimates the subsampled flow and subsequently enriches the particle concentration and 3) a thermodesorption unit (TD) heated at $T = 150^\circ \text{ C}$ that vaporises the particles prior their introduction into the drift tube. The PTR-ToF-MS is used with hydronium ions (H₃O⁺) to ionize organic analytes, and operates at a drift tube pressure of 2.6 mbar, a temperature of 120° C, and a voltage of 230 V. This results in an $E/N = 68 \text{ Td}$ (E = electric field, N = Number density of the gas molecules in the drift, 1 Td = $10^{-17} \text{ V cm}^2 \text{ molecule}^{-1}$). It represents a relatively low E/N compared to classical 120-140 Td
 125 reported in most of PTR-ToF-MS studies, as the aim is to minimise the potential fragmentation of parent ions and facilitate the molecular characterization of SOA. The potential higher dependence of the sensitivity to relative humidity variations at such low E/N can be neglected as all experiments were conducted at fixed relative humidity (Pang, 2015; Tani et al., 2003).



Instrument background has been daily performed using pure N₂, while sensitivity and particle enrichment factors (EF) are controlled at the end of the experiments. EF is determined by CHARON calibration using a vanillic acid solution based on the method recommended by Eichler et al. (2015). Instrument sensitivity is evaluated by calculating the transmission curve using a cylinder containing 14 gas standards (benzene, toluene, ethylbenzene, o-, m-, p-xylene, styrene, 1,2,4-trimethyl-, 1,3,5-trimethyl benzene, chloro-, 1,2-dichloro-, 1,3-dichloro-, 1,4-dichloro-, trichloro benzene, each at 100 ± 10%, ppb in N₂, RESTEK) covering a mass range up to m/z 181. IDA (Ionicon Data Analyzer 2.1.1.4) is used to process data recorded by the PTR-ToF-MS such as mass calibration, peak shape definition, peak identification and integration, rate constant calculation and VOC quantification (Müller et al., 2013). The peaks at m/z 21.022 (H₃¹⁸O⁺), m/z 330.847 corresponding to diiodobenzene (C₆H₅I₂⁺) and its fragment at m/z 203.943 (C₆H₅I⁺) are used to recalibrate the mass scale. Molecular formulas composed of C, H, O, N atoms are assigned based on exact mass position, chemical rules (valence of atoms, for example) and isotopic patterns. The molecular formula is used to calculate dipole moments and polarizability as introduced by (Bosque and Sales, 2002) and (Sekimoto et al., 2017), which allows to calculate k-rate constants based on the ion-molecule collision theories (Gioumousis and Stevenson, 1958; Langevin, 1950; Su and Chesnavich, 1982). Concentrations are then estimated based on the rate constant between a proton and each VOC, the experimental transmission of each compound, and the primary ion intensity. RStudio (RStudio 2023.06.0 Build 421) is used to perform a non-targeted approach for compound selection based on stability periods before and after oxidation. Time intervals are defined for each experiment corresponding to blank (photooxidation without VOC precursor, and HEPA (High-Efficiency Particulate Air) filter for particle phase), reactant (injection of products before the light has been turned on) and products (stable photooxidation), for both gas and particle phases. A Welch *t*-test is then used to statistically identify ions that are more concentrated than those in the blank. Then, among the selected ions, the products are defined as compounds more concentrated during oxidation period, and the invert for reactants, based also on Welch *t*-test. A high-resolution Time-of-Flight Aerosol Mass Spectrometer (HR-ToF-AMS, ToFwerk AG, Aerodyne Inc. USA) is employed for the quantification of the organic and inorganic aerosol fractions (Canagaratna et al., 2007; DeCarlo et al., 2006), with the data recorded by the AMS being analysed using the software SQUIRREL (ToF-AMS Analysis Toolkit 1.65C). The ionization efficiency (IE) with respect to nitrate anions was 4.58×10^{-8} . It was calculated using nebulised 300 nm mobility diameter ammonium nitrate particles (BFSP software). The relative IE (RIE) of ammonium was 3.45 based on the mass spectrum of ammonium nitrate data from IE calibrations. The RIE of sulphate was determined by comparing the theoretical and the measured concentration of a solution of ammonium nitrate and ammonium sulphate and was determined to be 1.75. For the organic fraction, the default value of 1.4 was used. The AMS data were corrected by collection efficiency (CE) calculated by comparison to the SMPS (Scanning Mobility Particle Sizer, TSI Classifier model 3082, DMA, TSI CPC 3776) volume using densities of 1.7 g cm⁻³ for ammonium sulphate and 1.4 g cm⁻³ for organics. The CE values varied from 0.3 for pure ammonium sulphate particles to 0.7 after SOA formation. The SMPS is used for measuring particle size distribution and number concentration. Additional instruments account for a chemiluminescent NO_x analyser (Envitec, model API200E), a pressure sensor (ATM.ECO, STS) and a temperature-humidity probe (HMP9 Vaisala) positioned close the aerosol flow tube outlet, the last two instruments being connected to a data logger (FieldLogger, NOVUS).

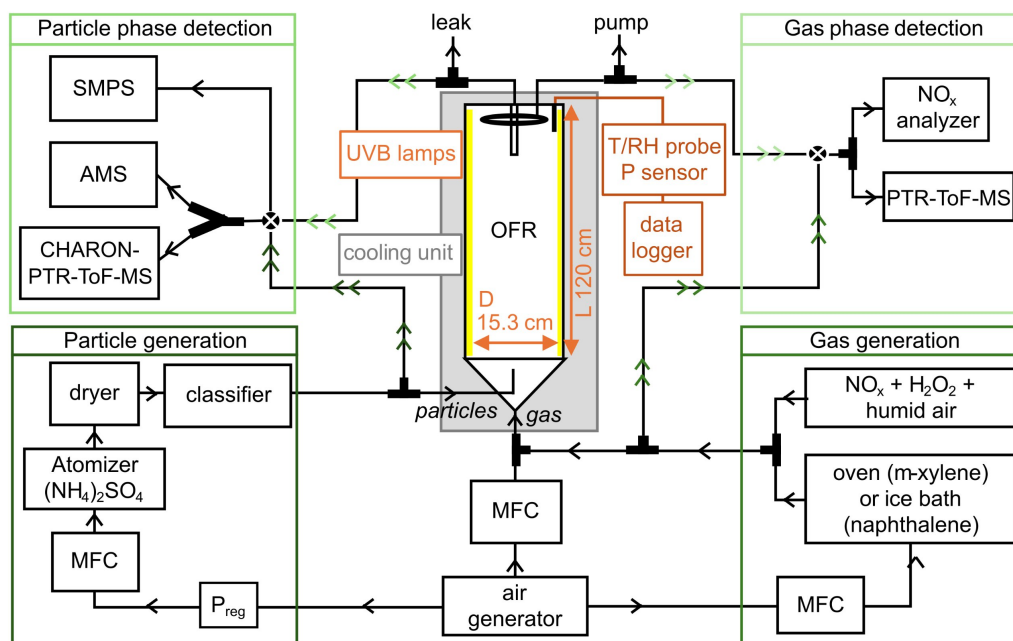


Figure 1. Schematic of the experimental setup.

2.3 SOA yield, partitioning, and volatility distribution

The expression to describe the fractional aerosol yield (Y) was established by (Odum et al., 1996, 1997) and is described in Eq. (1), where ΔM_0 is the amount of the total organic aerosol formed (in $\mu\text{g m}^{-3}$), and ΔVOC is the amount of VOC precursor reacted (in $\mu\text{g m}^{-3}$) measured as difference between inlet and outlet OFR.

$$Y = \frac{\Delta M_0}{\Delta VOC} \quad (1)$$

The distribution of oxidation products between gas and particle phase can be explained by the partitioning theory of (Yamasaki et al., 1982):

$$K_{p,i} = \frac{C_{p,i}}{C_{g,i} \times TSP} \quad (2)$$

where $K_{p,i}$ is the experimental partitioning coefficient (in $\text{m}^3 \mu\text{g}^{-1}$) of a species i , $C_{p,i}$ and $C_{g,i}$ are concentrations (in $\mu\text{g m}^{-3}$) of the species i in particle and gas phases, respectively, as measured by the CHARON-PTR-ToF-MS, and TSP is the total suspended particulate matter of the aerosol (in $\mu\text{g m}^{-3}$) as measured by SMPS. Larger K_p values indicate a preference for a compound to partition in the particle phase. Subsequently, the volatility of the species can be defined by $\log_{10} C_i^*$, where C_i^* is known as the effective saturation concentration (in $\mu\text{g m}^{-3}$) of a species i and calculated as the reciprocal of $K_{p,i}$ (Donahue et al., 2011):



$$C_i^* = \frac{1}{K_{p,i}} \quad (3)$$

180 The estimated values have been calculated using Volcalc model based on molecular properties such as molecular weight, numbers of atoms and functional groups (Meredith et al., 2023; Riemer, 2023). The model is based on SIMPOL.1 method (Pankow and Asher, 2008), which implements a structure–activity relationship method to calculate the subcooled pure liquid vapor pressure by summing the contributions of the subcooled liquid vapor pressures of individual chemical functional groups:

$$\log_{10} P_{L,i}^{\circ}(T) = \sum_k v_{k,i} b_k(T) \quad (4)$$

185 where $P_{L,i}^{\circ}(T)$ is the liquid vapor pressure (atm), $v_{k,i}$ is the number of groups of type k in i , the index k can take on the entire numbers (1,2,3, etc.), and $b_k(T)$ is the group contribution term for group k . No second-order interaction terms are included to account for neighbouring functional groups, which means that the model does not consider the potential interactions or effects that adjacent functional groups might have on each other but only sums the contributions of individual functional groups independently.

190 The saturation concentration (C_i°) of the major identified species is calculated at 280 and 295 K as follows:

$$C_{i,T}^{\circ} = C_{i,293}^{\circ} \times \frac{293}{T} \times \exp\left(\left(\frac{-\Delta H}{R}\right) \times \left(\frac{1}{T} - \frac{1}{293}\right)\right) \quad (5)$$

The saturation concentration (C_i°) and the effective saturation concentration (C_i^*) are related through the activity coefficient (g_i) that captures the non-ideal interactions of the compound with the aerosol mixture. Its value generally lies between 0.3 (readily partitions to particle phase) and 3 (readily partitions to gas phase) for ambient atmospheric aerosol (Donahue et al., 2011; Liu et al., 2021). As in previous studies, such as Isaacman-VanWertz et al. (2016) and Nie et al. (2022), in this work we assume a g value of 1.

3 Results and discussion

3.1 SOA yield formation

200 Table 1 summarizes experimental conditions, consumed reactants (ΔVOC) and formed organics (ΔM_0) used to calculate the SOA yield (Y) for each experiment (Eq. (1)). Figure 2 presents SOA yields for (a) m-xylene and (b) naphthalene, comparing them with results from previous studies (Chan et al., 2009; Chen et al., 2018; Ng et al., 2007; Song et al., 2005). Filled markers indicate high NO_x conditions ($VOC/NO_x < 8$), empty markers refer to low NO_x conditions ($VOC/NO_x > 8$) (Dodge, 1977; NARSTO. and Electric Power Research Institute., 2000). The red square and blue triangle markers refer to this study at 295 K and 280 K, respectively, while all other experiments are conducted at room temperatures (between 295 K and 300 K).

205



Table 1. List of conducted laboratory experiments and associated conditions, such as OFR temperature, RH, VOC/NO_x ratio, seeds mass and SOA yield.

	T	RH	VOC	NO _x	VOC/NO _x	Seeds	[OH] × 10 ⁷	ΔVOC	ΔM ₀	Y
	K	%	ppbV	ppb	ppbC ppb ⁻¹	μg m ⁻³	molecules cm ⁻³	μg m ⁻³	μg m ⁻³	%
m-xylene	280	65	74	222	2.7	51	3.5	114	26.4	23.1
	280	50	69	40	13.9	35	2.3	95	26.1	27.5
	295	60	73	221	2.6	30	5.4	155	12.6	8.1
	295	55	83	40	16.6	34	4.7	153	21.1	13.8
naphthalene	280	40	74	340	2.2	46	3.1	92	23.3	25.3
	280	35	78	62	12.6	36	3.5	79	33.6	42.7
	295	40	70	340	2.1	55	3.5	84	12.6	14.9
	295	50	67	57	11.8	65	3.1	75	13.8	18.3

210 For m-xylene (Fig. 2a), the SOA yield at 295 K under high NO_x condition is approximately 8 % (filled red square) in agreement with reported values by Ng et al. (2007) and Chen et al. (2018). Ng et al. (2007) conducted experiments with AS seeds, using nitrous acid (HONO) as precursor for OH, with initial xylene concentrations from 42 to 171 ppb that may explain the SOA yields variability (from 3 to 8 %). Chen et al. (2018) reported similar SOA yields in the absence of seeds but used higher VOC/NO_x ratios and slightly lower precursor concentrations (44-59 ppb). Lower initial levels of the VOC precursor increase
 215 the amount of S/IVOCs (Chen et al., 2019), whereas the absence of seeds reduces the available surfaces during the first steps of the experiment (Ahlberg et al., 2019; Lambe et al., 2015). But both studies were conducted in dry conditions. Li et al. (2022) reported SOA yields increasing from 6.3 to 14 % when humidity increased from 10 % to 70 %. The order of magnitude of SOA yields in this study is close to what we observed, the variability of yields being associated mostly to NO_x or NH₃ initial concentrations. Under low NO_x, a SOA yield of 14 % (empty red square) is observed, lying on the lower level (12-30 %) of
 220 reported values by Song et al. (2007), that used lower levels of xylene (39-52 ppb).

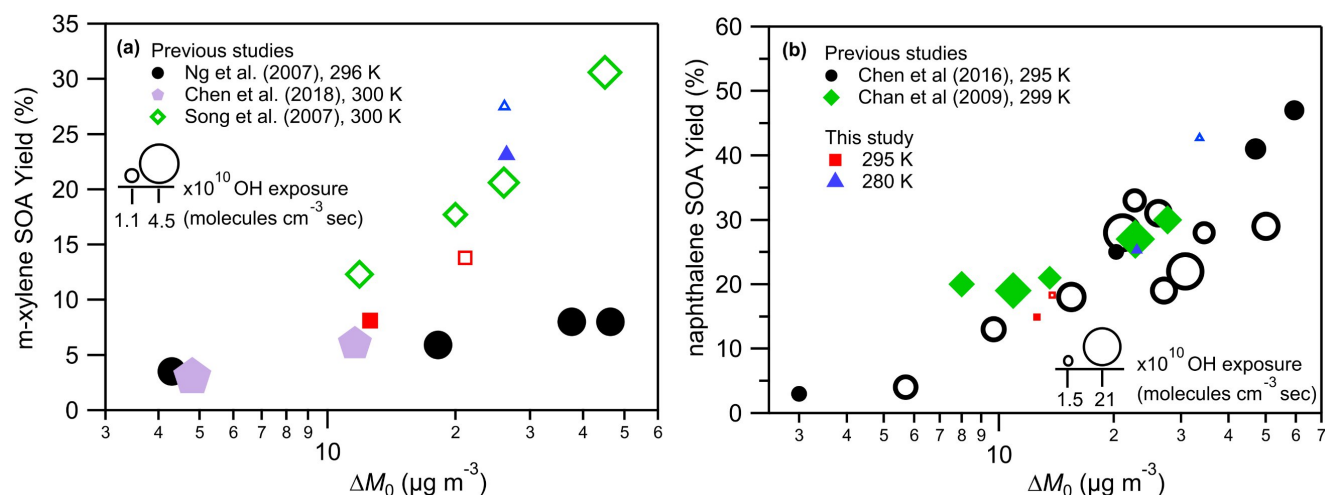


Figure 2. SOA yields at 295 K and 280 K as function of organic aerosol mass formed for (a) m-xylene and (b) naphthalene in comparison with previous studies. Filled markers correspond to high NO_x conditions, open markers to low NO_x . The size of the markers is proportional to OH exposure (molecules cm^{-3} sec).

225 The effect of temperature on SOA yield is also depicted in Fig. 2. When decreasing from 295 K to 280 K, SOA yield increases from 8 to 23 % under high NO_x conditions and from 14 to 28 % under low NO_x conditions. Only a few studies investigated the role of low temperature on SOA formation from monoaromatic precursors. Regarding xylene, only Takekawa et al. (2003) reported that SOA yield is enhanced by a factor around 2 (from 6 % to 13 %, on average) when temperature decreases from 303 K to 283 K at a VOC/ NO_x around 10 (like low NO_x conditions in this study). This is in good agreement with our results, where a decrease of 15 K doubles the SOA yield under low NO_x conditions (Fig. 2). Lannuque et al., (2023) found a similar temperature dependence of toluene-SOA and highlighted that the effect was greater for low concentrations of the precursors.

For naphthalene (Fig. 2b), SOA yield at 295 K with high NO_x conditions ranges from 15 to 18 %, in agreement with Chen et al. (2016) and Chan et al. (2009) that reported values from 3 % to 47 %. Chen et al. (2016) observed the lowest yield under high NO_x , attributed to the lowest amount of OH generated and highest NO injection. Even though Chan et al. (2009) used AS seeds, the initial amount of naphthalene was less than half of that used in our experiments and the humidity was below 10 %, highlighting again the important effect of experimental conditions on the prediction of SOA yields. Lower naphthalene SOA yields are generally observed under high NO_x conditions (filled vs empty square or triangle, Fig. 2). Under low NO_x conditions, a yield of 18 % is observed in quite good agreement with Chen et al. (2016), that reported yields varying from 4 % to 29 % as a function of the VOC/ NO_x ratio, with lowest yields for highest NO_x regimes. A consistent increase in SOA yield is observed when switching from high to low NO_x regime at 280 K, from 25 to 43 % at 280 K, while at 295 K the variation is limited to few percent increase. The presence of NO_x in the system may promote a competition for the termination reaction of RO_2 radicals between peroxy radicals (RO_2 and HO_2) and NO_x (NO_2 and NO), leading to less oxidised products of higher volatility (Henze et al., 2008; Kroll and Seinfeld, 2008).

The effect of temperature on naphthalene SOA is reported here for the first time, and it is slightly lower compared to the m-xylene SOA system. Reducing the experimental temperature from 295 K to 280 K induces an increase from 14.9 % to 25.3 % for high NO_x conditions, and from 18.3 % to 42.7 % for low NO_x conditions. SOA yields from naphthalene are in general higher compared to m-xylene, which is expected considering larger carbon skeleton of naphthalene (Aumont et al., 2013; La et al., 2016) and is in good agreement with previous studies (Chan et al., 2009; Chen et al., 2018).

3.2 Chemical composition of oxidation products in gas and particle phases

3.2.1 m-xylene

Figure 3 presents the chemical distribution of gas (Fig. 3a) and particle (Fig. 3b) phase products as a function of the carbon atoms following m-xylene oxidation by OH radicals. The mass fraction (in $\mu\text{g m}^{-3}$) is further sub-classified based on the number of oxygen atoms (according to colour scale), and the molecular weight distribution was divided into three groups: *m/z* below 100, *m/z* 101-150, and *m/z* above 150. The experiment has been carried out under high NO_x at 280 K. The total m-xylene carbon balance varies within 26-48 % for the detected gas phase products depending on the oxidation conditions and considering that CO, CO₂ and glyoxal are not measured. The latter compound has strong interferences with the high signal of acetone. The SOA formed corresponds to 2.5 % of the total carbon balance at 295 K and 7 % at 280 K under high NO_x conditions.

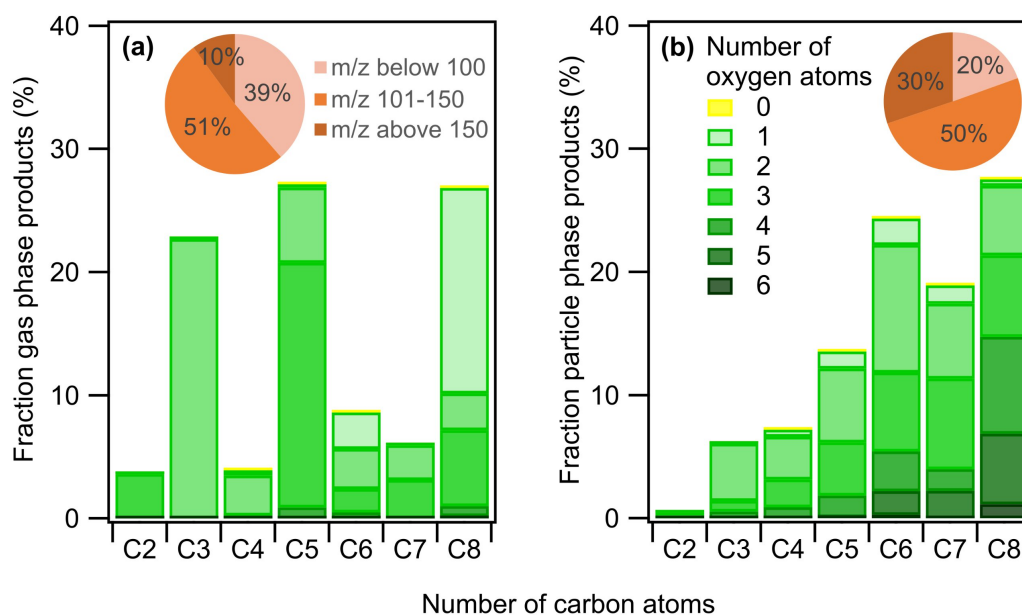


Figure 3. m-xylene mass products fraction (y-axis) distribution based on the number of carbon atoms (x-axis) for a high NO_x experiment 280 K, coloured by the number of oxygen atoms. Detected compounds are in the (a) gas phase and (b) particle phase. Pie charts correspond to the molecular weight contribution to the overall mass.



The overall product distribution at 295 K is similar to that at 280 K and can be found in the SI section (Figs. S1a and S1b). At both temperatures, the gas phase is mainly composed of C₃, C₅ and C₈ products with 1 to 3 O atoms for most of them, while the particle phase is dominated by C₆, C₇ and C₈ compounds, containing generally 2 to 5 O atoms. In the gas phase, C₈ compounds are ring retaining compounds related to first-generation products, while C₃ and C₅ products arise from a more advanced chemistry. A larger fraction of C₃ products is present at 295 K when compared to 280 K (Figs. 3 and S1a). This could be due to the higher OH concentration for the experiment at 295 K (Table 1), leading to a higher consumption of C₆ and C₈ oxidation products due to their faster reactivity. This is supported by the time evolution of some compounds such as C₆H₈O at *m/z* 97.06, C₆H₆O₂ at *m/z* 111.04, C₆H₈O₄ at *m/z* 145.05, C₈H₁₀O₅ at *m/z* 187.06 (Fig. S3). This hypothesis is also backed up by previous studies reporting the reaction of oxidation products (Cappa and Wilson, 2012; Isaacman-VanWertz et al., 2018; Jin et al., 2021). While for experiments with lower OH concentration, as at 280 K, the gas phase products (Fig. 3a) are characterised by a higher fraction of C₈ (26%) and C₅ (27%) compounds.

The condensed phase is enriched in compounds with higher molecular weight when compared to the gas phase, along with the presence of four or more oxygen atoms which highly reduces their vapour pressure (Cappa and Wilson, 2012). Particle phase products generally exhibit an increasing trend from C₁ to C₈ (Fig. 3b), similar to a recent study on toluene SOA (Lannuque et al., 2023).

Table 2 lists identified ions from the gas and particle phase products for two experiments at high NO_x at 295 K and 280 K. The columns present the measured *m/z* signals, the attributed chemical formula and a tentative chemical assignment based on results from previous studies on *m*-xylene photooxidation (Atkinson et al., 1991; Forstner et al., 1997; Huang et al., 2008; Jang and Kamens, 2001; Li et al., 2018, 2022; Zhang et al., 2019a, b; Zhao et al., 2005) and on the CHARON assignment procedure recommended by Gkatzelis et al. (2018) where average saturation mass concentration log₁₀(C_i^{*}) are used to discriminate between parent and fragment ions. The compounds are sorted in decreasing numbers of carbon atoms. For each temperature, two columns are presented: the first indicates the contribution of each compound to total gas phase organic products and the second the contribution to SOA.

Table 2. Ions and their corresponding formulas of the major *m*-xylene products detected during photooxidation experiments under high NO_x. Reaction products are given as a fraction of the gas phase products (in % of μg m⁻³) and as a fraction of the SOA products (in % of μg m⁻³).

Carbon number	Measured <i>m/z</i> and ion sum formula	Tentative assignment	<i>T</i> = 298 K		<i>T</i> = 280 K	
			Gaseous Products (%)	SOA Products (%)	Gaseous Products (%)	SOA products (%)
8	121.06 (C ₈ H ₈ O)H ⁺	<i>m</i> -tolualdehyde	13.9	0.6	16.7	0.5
8	155.07 (C ₈ H ₁₀ O ₃)H ⁺	dimethyl-epoxy-oxo-hexenal/ trihydroxy dimethyl benzene	n.d.	3.8	n.d.	3.3
8	137.06 (C ₈ H ₈ O ₂)H ⁺	toluic acid and possible contribution frag. 155.07	n.d.	8.5	n.d.	5.7
8	171.07 (C ₈ H ₁₀ O ₄)H ⁺	dihydroxy-dimethyl-cyclohexenedione /	0.3	4.6	0.3	5.6



		dimethyl-hexadienedioic acid				
8	153.06 (C ₈ H ₈ O ₃)H ⁺	hydroxy dimethyl quinone	1.9	2.8	2.4	2.9
8	187.06 (C ₈ H ₁₀ O ₅)H ⁺	hydroxy-cyclohexene-dicarboxylic acid oxo-cyclohexanedicarboxylic acid	0.1	2.6	0.1	2.5
8	169.05 (C ₈ H ₈ O ₄)H ⁺	dihydroxy-methylbenzoic acid	n.d.	2.0	n.d.	1.6
8	185.05 (C ₈ H ₈ O ₅)H ⁺	trihydroxy-(hydroxymethyl)benzaldehyde	n.d.	1.0	n.d.	0.7
8	168.06 (C ₈ H ₉ NO ₃)H ⁺	<i>dimethyl nitrophenol</i>	1.9	0.4	3.6	0.4
8	152.07 (C ₈ H ₉ NO ₂)H ⁺	<i>nitro-xylene</i>	0.4	0.1	1.8	0.1
7	125.06 (C ₇ H ₈ O ₂)H ⁺	dimethyl-pyranone/ methyl-hexadienedial	n.d.	3.6	1.6	5.0
7	141.05 (C ₇ H ₈ O ₃)H ⁺	methyl-oxo-hexadienoic acid /heptenetrione	0.7	2.8	0.7	4.0
7	139.04 (C ₇ H ₆ O ₃)H ⁺	hydroxy benzoic acid/ hydroxy methyl benzoquinone	n.d.	3.1	n.d.	2.4
7	157.05 (C ₇ H ₈ O ₄)H ⁺	hydroxy-dioxo-heptenal / epoxymethylhexenedial	n.d.	2.0	n.d.	1.8
7	109.06 (C ₇ H ₈ O)H ⁺	cresols/ benzyl alcohol	n.d.	1.4	n.d.	1.5
7	173.06 (C ₇ H ₈ O ₅)H ⁺	hydroxy-dioxo-heptenoic acid	n.d.	1.8	n.d.	1.2
7	138.06 (C ₇ H ₇ NO ₂)H ⁺	<i>nitrotoluene</i>	1.1	0.4	1.2	0.3
7	154.05 (C ₇ H ₇ NO ₃)H ⁺	<i>nitrocresol</i>	0.7	0.3	0.6	0.3
6	127.04 (C ₆ H ₆ O ₃)H ⁺	hydroxymethyl furfural/ hydroxyquinol/dimethylfuranone	1.0	2.4	1.4	3.3
6	113.06 (C ₆ H ₈ O ₂)H ⁺	methyl-oxo-pentenal / dimethylfuranone	n.d.	1.7	0.2	2.2
6	129.06 (C ₆ H ₈ O ₃)H ⁺	hydroxy-oxo-hexenal methyl-oxo-pentenoic acid	0.4	1.6	0.4	2.7
6	111.04 (C ₆ H ₆ O ₂)H ⁺	methylfuraldehyde / benzenediols possible frag. of 129.06	n.d.	3.6	2.7	6.2
6	143.03 (C ₆ H ₆ O ₄)H ⁺	dioxo-hexenoic acid/ methyl-dioxo- pentenoic acid tetrahydroxybenzene	n.d.	1.4	0.2	1.8
6	159.04 (C ₆ H ₆ O ₅)H ⁺	oxo-hexenedioic acid	n.d.	1.2	n.d.	1.2
6	145.05 (C ₆ H ₈ O ₄)H ⁺	hydroxy-dioxo hexanal	n.d.	1.2	0.1	1.1
6	115.07 (C ₆ H ₁₀ O ₂)H ⁺	cyclopentylcarboxylic acid	n.d.	0.4	0.4	1.1
6	95.03 (C ₆ H ₆ O)H ⁺	phenol	n.d.	1.4	n.d.	1.2
5	113.02 (C ₅ H ₄ O ₃)H ⁺	methyl-furanone	16.7	1.3	19.3	2.1
5	131.04 (C ₅ H ₆ O ₄)H ⁺	methy-hydroxy-oxo-butandial	2.1	1.4	0.9	0.9
5	117.05 (C ₅ H ₈ O ₃)H ⁺	oxo-pentanoic acid + frag at 99.04	1.2	0.7	0.2	0.4
	99.04 (C ₅ H ₆ O ₂)H ⁺	oxo-pentenal / methyl-butendial	6.7	3.5	2.8	3.9
5	115.03 (C ₅ H ₆ O ₃)H ⁺	oxo-pentenoic acid	1.4	2.4	0.7	1.8
5	97.03 (C ₅ H ₄ O ₂)H ⁺	furaldehyde	1.1	0.7	2.2	1.7
5	101.06 (C ₅ H ₈ O ₂)H ⁺	oxo-pentanal and isomers + frag at 83.05	n.d.	0.4	n.d.	0.4
	83.05 (C ₅ H ₆ O)H ⁺	methylfuran	0.6	1.0	0.3	1.3
4	71.05 (C ₄ H ₆ O)H ⁺	dihydrofuran / MACR / MVK	1.1	0.3	0.4	0.3
4	87.04 (C ₄ H ₆ O ₂)H ⁺	butanedial / crotonic acid	n.d.	2.0	n.d.	2.2
4	103.04 (C ₄ H ₆ O ₃)H ⁺	hydroxy-oxo-butanal	0.4	1.5	0.1	1.3
4	85.03 (C ₄ H ₄ O ₂)H ⁺	butenedial	n.d.	1.3	n.d.	1.2



3	73.03 (C ₃ H ₄ O ₂)H ⁺	methylglyoxal	20.9	3.2	9.5	2.7
3	75.04 (C ₃ H ₆ O ₂)H ⁺	propanoic acid	14.3	1.7	13.3	1.6
3	89.02 (C ₃ H ₄ O ₃)H ⁺	pyruvic acid / hydroxy-propanedial	1.5	0.6	n.d.	0.6
2	77.03 (C ₂ H ₄ O ₃)H ⁺	PAN fragment	3.7	0.3	3.6	0.5

290 *n.d. = not detected

The C₈ compounds are dominating both gas and particle phases accounting for 27 % of the total products. The most abundant C₈ gas phase product is m-tolualdehyde (C₈H₈O detected at *m/z* 121.06), comprising alone 17 % of the reaction products. It is a first generation ring-retaining aromatic compound previously identified in many studies (Atkinson et al., 1991; Forstner et al., 1997; Huang et al., 2008; Srivastava et al., 2023; Zhang et al., 2019b; Zhao et al., 2005). Toluic acid is a second generation ring retaining compound formed by the additional oxidation of m-tolualdehyde by OH radical (Forstner et al., 1997; Srivastava et al., 2022, 2023), and it is a major C₈ particle phase product (C₈H₈O₂, detected at *m/z* 137.06) contributing to 5 % of the SOA mass. Another major SOA component is found at *m/z* 171.07 (C₈H₁₀O₄) tentatively assigned to dimethyl-hexadienedioic acid, a ring opening product possibly formed by OH-addition to the benzene ring followed by a ring cleavage, or to dihydroxy-dimethyl-cyclohexenedione, a ring retaining compound formed by successive OH radical reactions on the benzene ring. A second ring opening compound is detected at *m/z* 155.07 (C₈H₁₀O₃) previously identified as dimethyl-epoxy-oxo-hexenal (Zhao et al., 2005). Other C₈ compounds are C₈H₈O₃₋₅ (at *m/z* 153.06, *m/z* 169.05 and *m/z* 185.05) and C₈H₁₀O₅ at *m/z* 187.06 (Table 2).

The contribution of C₇ compounds to gas and particle phases accounts for 6 % and 19 %, respectively. Among the C₇ prominent products in the particle phase we identify C₇H₈O₂ at *m/z* 125.06 tentatively assigned to dimethyl-pyranone (Forstner et al., 1997) or methyl-hexadienedial resulting from a ring opening of the phenoxy radical intermediate formed via OH-addition to the ring (Jang and Kamens, 2001). Further oxidation of methyl-hexadienedial will result in methyl-oxo-hexadienoic acid C₇H₈O₃ at *m/z* 141.05 (Jang and Kamens, 2001). Another C₇ compound is the C₇H₆O₃ at *m/z* 139.04 tentatively assigned to methyl cyclohexene tricarbonyls or hydroxy methyl benzoquinone, both being ring-retaining products. They can be formed upon OH-addition to first- or second-generation products and release of one methyl group (Jang and Kamens, 2001). Other C₇ compounds important in the particle phase include C₇H₈O (detected at *m/z* 109.06), C₇H₈O₄ (detected at *m/z* 157.05), and C₇H₈O₅ (detected at *m/z* 173.04). Some of the C₇-C₈ products are nitrogen containing-compounds: nitro-m-xylene (C₈H₉NO₂, at *m/z* 152.07), nitrotoluene (C₇H₇NO₂ at *m/z* 138.06), dimethyl nitrophenol (C₈H₉NO₃ at *m/z* 168.06) and nitrocresol (C₇H₇NO₃ at *m/z* 154.05). The latter is the result of NO₂ reaction with the benzyl peroxy radical in the H-abstraction route (Li et al., 2018; Srivastava et al., 2023). Aliphatic nitrogen-containing compounds are easily fragmented in the PTR-MS and thus are hardly detected. Nevertheless, a known peroxyacetyl nitrate (PAN) fragment C₂H₄O₃ detected at *m/z* 77.03, also previously assigned as an unspecific fragment from nitro-group containing compounds has been detected (Müller et al., 2012). In total, the sum of all nitrogen-containing products (including PAN fragment) accounted for 9-14 % of the gaseous phase mass loading



and 6 % of the particulate phase under high-NO_x conditions, which is close to what was seen in toluene photooxidation experiments by Lannuque et al. (2023).

The C₆ compounds accounted for only 6 % of the gas phase and for 19% of the organic aerosol fraction. Top products are ring-retaining furan-derived, such as methyl-furaldehyde or benzenediols (C₆H₆O₂, detected at *m/z* 111.04) making up 3 % and 6 % in gas and particle phases respectively, and dimethylfurandione (C₆H₆O₃, detected at *m/z* 127.04) with 1.4 % in the gas phase, and 3.3 % in the particle phase, alongside with dimethyl-furanone with 2.2 % in the particle phase (C₆H₈O₂, detected at *m/z* 113.06). Furanoid products can be formed through a bridged oxide intermediate on a bicyclic ring whereas furandiones are known to originate from conjugated dicarbonyls via reaction with OH-radicals followed by cyclization (Forstner et al., 1997; Jang and Kamens, 2001). Examples of unsaturated dicarbonyls and tricarbonyls in the condensed phase are methyl-oxo-pentenal (C₆H₈O₂, detected at *m/z* 113.06), and hydroxy-oxo-hexenal (C₆H₈O₃, detected at *m/z* 129.06), also assigned to methyl-oxo-pentenoic acid (Li et al., 2017, 2018; Zhao et al., 2005). Those multi-carbonyls are a result of the decomposition of bicyclic alkoxy radicals (Huang et al., 2008; Zhao et al., 2005). Other C₆ compounds can be found at *m/z* 143.03 (C₆H₆O₄), 97.06 (C₆H₈O), 145.05 (C₆H₈O₄), and 115.07 (C₆H₁₀O₂) (Table 2).

As shown in Fig. 3 and Fig. S1, the C₅ products represent a major contributor of the gas phase with around 30 % of the total organic gaseous products and 13 % of the particle phase. In agreement with previous studies, most of the compounds are furan derivatives (Forstner et al., 1997; Jang and Kamens, 2001; Li et al., 2018). The C₅H₄O₃ (detected at *m/z* 113.02) assigned to methylfurandione accounts alone for, 17-19 % of the gas phase products, followed by oxo-pentenal and isomers (C₅H₆O₂, detected at *m/z* 99.04) with 3-7 % abundance. Other important products include unsaturated or oxo-aldehydes (such as C₅H₆O₂ at *m/z* 99.04 and C₅H₆O₄ at *m/z* 131.04), organic acids such oxo-pentenoic acid (C₅H₆O₃ at *m/z* 115.03) (Table 2). Lannuque et al. (2023) identified dihydroxy-oxopentanoic acid (DHOPA, C₅H₈O₅), a known tracer of toluene and xylene SOA, in particle phase. In our study, DHOPA parent ion was below the detection limit which is highly probable considering its very low formation yield (Srivastava et al., 2023) and the low precursor concentration used compared to Lannuque et al. (2023). We therefore assume that DHOPA did not contribute significantly to the fragment ion at *m/z* 131.04 (C₅H₆O₄) expected upon water loss. In general the high contribution of C₅ compounds can be explained by the *m*-xylene structure (C₈ aromatic) and the presence of two methyl groups on the benzene ring, which implies the formation of methylated furan derivatives such as methyl-furandione, methyl-furanone and furaldehyde, in addition to the high contribution of C₃ compounds such as methylglyoxal, in agreement with previous studies (Birdsall and Elrod, 2011; Fan and Zhang, 2008; Forstner et al., 1997; Jang and Kamens, 2001; Li et al., 2022; Song et al., 2007; Zhang et al., 2019b).

The C₄ compounds are the least abundant in both phases (below 7 %, on average) and account for shorter functionalized aldehydes, furans and acids formed by minor pathways in the aromatic ring cleavage (Table 2). This is in agreement with the above explained ring opening mechanism, that mainly breaks the carbon skeleton of the xylene in C₅ and C₃ compounds, instead of two C₄ moieties (Forstner et al., 1997; Jenkin et al., 2003; Pan and Wang, 2014).

The C₃ compounds account for 23-37 % of the gas phase and 6 % of the particle phase products. Methylglyoxal (C₃H₄O₂, detected at *m/z* 73.03) accounts for 21% of the gas phase products at 295 K while it is close to 10 % at 280 K. It makes up to

3 % of the SOA fraction and is a major second-generation product resulting from the ring cleavage of bicyclic alkoxy radicals (Fan and Zhang, 2008). Propanoic acid ($C_3H_6O_2$, detected at m/z 75.04) accounts for 8 % of the gaseous phase and only 1 % in the particle phase, as it is a quite volatile compound. This reaction product can result from the oxidation of multifunctional ring opening products (Jang and Kamens, 2001).

3.2.2 Naphthalene

In analogy with the m-xylene, Fig. 4 presents the chemical distribution of naphthalene gas phase products (Fig. 4a) and particle phase products (Fig. 4b) for photooxidation experiments under high NO_x conditions at 280 K, in addition to pie charts showing the molecular weight distribution. Out of the total naphthalene carbon balance, 30-32 % is accounted for the detected gas phase products under the different oxidation conditions, taking into account that CO, CO_2 and glyoxal are not measured. As for the SOA formed, it corresponds to 8 % at 295 K and 14 % at 280 K of the carbon balance under high NO_x conditions.

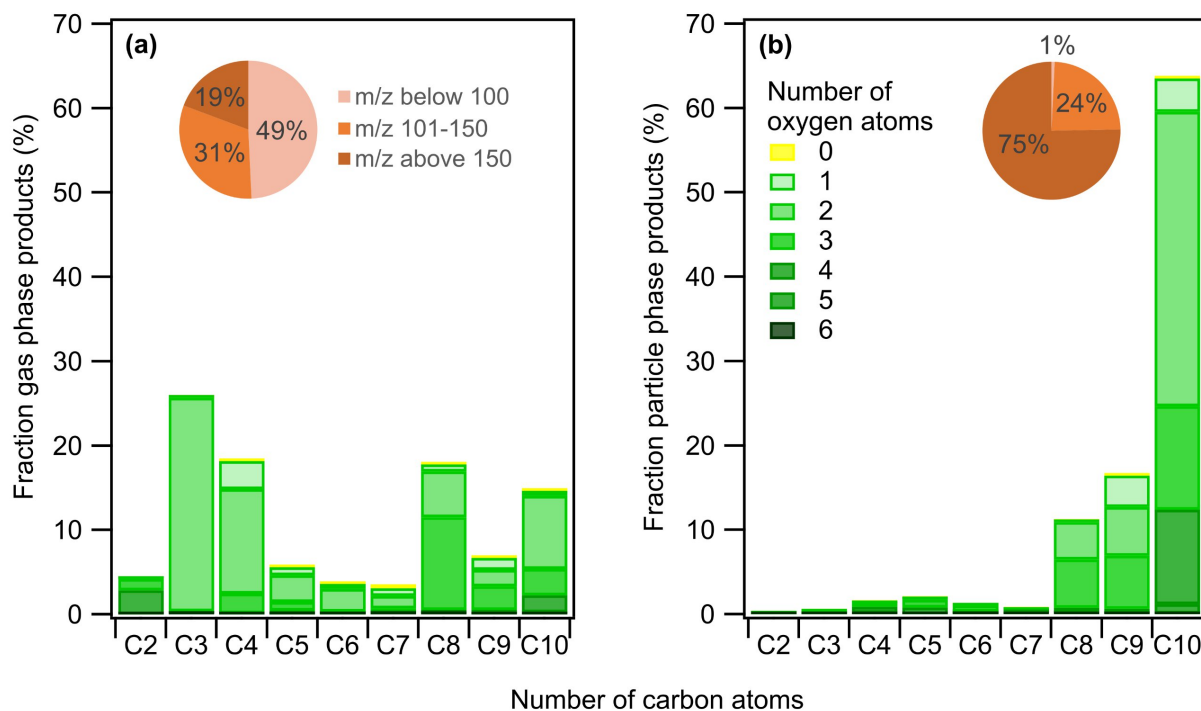


Figure 4. Naphthalene mass products fraction (y-axis) distribution based on the number of carbon atoms (x-axis) for a high NO_x experiment 280 K, coloured by the number of oxygen atoms. Detected compounds are in the (a) gas phase and (b) particle phase. Pie charts correspond to the molecular weight contribution to the overall mass.

As the measured carbon distribution is comparable at the two temperature conditions, only the experiment at 280 K is shown in the main text (see Fig. S2 for distributions at 295 K). The gas phase products distribution is dominated by C_{10} and C_8 compounds containing mainly 2 or 3 oxygen atoms followed by C_3 and C_4 compounds, such as methylglyoxal, resulting from the further degradation of naphthalene oxidation products. As expected, the particle phase contains more oxygen atoms and is



375

characterized by heavy molecular weight compounds with m/z above 150 comprising 75 % of the overall mass, explained by the readily partitioning of major C_{10} products containing mainly 2 to 4 oxygen atoms. Table 3 presents the major identified ion fragments, their corresponding chemical formula and a tentative assignment to each compound based on previous studies (Bunce et al., 1997; Chan et al., 2009; Chen et al., 2016; Kautzman et al., 2010; Lee and Lane, 2009; Nishino et al., 2009; Riva, 2013; Sasaki et al., 1997; Tomaz, 2015).

Table 3. List of ions and their corresponding formulas of the major naphthalene products detected during photooxidation experiments under high NO_x . Reaction products are given as fraction of the gas phase products (in % of $\mu g\ m^{-3}$) and as fraction of the SOA products (in % of $\mu g\ m^{-3}$).

Carbon number	Measured m/z and ion sum formula	Tentative assignment	$T = 295\ K$		$T = 280\ K$	
			Gaseous products (%)	SOA products (%)	Gaseous products (%)	SOA products (%)
10	161.06 ($C_{10}H_8O_2$) H^+	formyl cinnamaldehyde	2.0	8.9	3.5	25.4
10	193.05 ($C_{10}H_8O_4$) H^+	carboxy cinnamic acid	0.8	15.3	1.0	8.1
10	159.04 ($C_{10}H_6O_2$) H^+	naphthoquinone	6.6	5.6	4.9	9.3
10	177.05 ($C_{10}H_8O_3$) H^+	formyl cinnamic acid	0.6	7.7	1.1	7.1
10	175.04 ($C_{10}H_6O_3$) H^+	epoxy-naphthoquinone	1.6	8.4	1.9	4.8
10	145.07 ($C_{10}H_8O$) H^+	naphthol	0.4	2.2	0.5	3.6
10	191.04 ($C_{10}H_6O_4$) H^+	dihydroxy naphthoquinone	0.7	3.5	0.8	2.0
10	195.06 ($C_{10}H_{10}O_4$) H^+	carboxybenzenepropanoic acid benzofurancarboxyaldehyde	0.3	1.5	0.3	1.0
10	174.05 ($C_{10}H_7NO_2$) H^+	<i>nitronaphthalene</i>	1.2	0.3	0.3	0.2
10	190.05 ($C_{10}H_7NO_3$) H^+	<i>nitronaphthol</i>	0.5	2.5	0.1	0.4
9	147.05 ($C_9H_6O_2$) H^+	benzopyrone	3.5	8.3	1.9	5.8
9	163.04 ($C_9H_6O_3$) H^+	hydroxycoumarin	1.5	6.3	2.2	4.5
9	133.06 (C_9H_8O) H^+	indanone	1.6	1.3	1.3	3.6
9	179.04 ($C_9H_6O_4$) H^+	dihydroxy-indanedione	0.5	4.2	0.1	2.8
9	165.06 ($C_9H_8O_3$) H^+	hydroxy cinnamic acid	0.9	2.7	0.6	1.8
9	181.05 ($C_9H_8O_4$) H^+	dihydroxy cinnamic acid	0.2	1.5	0.2	0.9
8	135.05 ($C_8H_6O_2$) H^+	phthaldialdehyde / phthalide	19.3	3.9	5.4	4.3
8	149.03 ($C_8H_4O_3$) H^+	phthalic anhydride	13.8	3.3	9.9	2.0
8	151.04 ($C_8H_6O_3$) H^+	hydroxy phthaldehyde hydroxy phthalide	0.5	1.2	1.0	3.7
7	123.05 (C_7H_6O) H^+	benzoic acid	1.9	0.2	1.4	0.1
7	107.05 (C_7H_6O) H^+	benzaldehyde	1.0	n.d.	0.9	n.d.
6	111.05 ($C_6H_6O_2$) H^+	catechol / benzoquinone	1.2	n.d.	0.9	n.d.
6	115.07 ($C_6H_{10}O_2$) H^+	dimethyloxolan-one / hexanedione	1.3	0.3	1.3	0.6
5	101.06 ($C_5H_8O_2$) H^+	methyl furan	0.7	n.d.	1.6	n.d.



4	89.06 (C ₄ H ₈ O ₂)H ⁺	hydroxybutanone / hydroxybutanal	10.1	0.1	11.5	n.d.
4	71.05 (C ₄ H ₆ O)H ⁺	dihydrofuran / MACR / MVK	1.2	n.d.	1.8	n.d.
3	75.04 (C ₃ H ₆ O ₂)H ⁺	propanoic acid	12.3	0.3	19.9	0.2
3	73.03 (C ₃ H ₄ O ₂)H ⁺	methylglyoxal	3.6	0.1	5.4	0.1
2	77.02 (C ₂ H ₄ O ₃)H ⁺	PAN fragment	2.0	0.1	1.3	0.1

*n.d. = not detected

The C₁₀ compounds account for around 15 % of the gas phase products at both temperatures and clearly dominate the particulate phase with 59 % and 64 % of the overall aerosol mass at 295 K and 280 K, respectively. The 2-formyl cinnamaldehyde (C₁₀H₈O₂ at *m/z* 161.06) is the most abundant particle phase product accounts for 25 % of the SOA formed at 280 K. It is assumed to be formed via two possible routes i) ring cleavage upon the reaction of the naphthol peroxy radical (from an OH-naphthalene adduct) with NO, and ii) a hydrogen shift from the alcohol group on the naphthol peroxy radical followed by loss of OH and ring opening (Kautzman et al., 2010; Nishino et al., 2009; Qu et al., 2006; Sasaki et al., 1997; Wang et al., 2007). The predominance of one route over the other is depending on the amount of NO_x. The 2-formyl cinnamaldehyde can further be oxidised, leading to the formation of 2-carboxy cinnamic acid (C₁₀H₈O₄ at *m/z* 193.05), the second most important C₁₀ compound that accounts for 8-15 % of the SOA mass. The oxidation of 2-formyl cinnamaldehyde also produces 2-formyl cinnamic acid (C₁₀H₈O₃ at *m/z* 177.05) (Bunce et al., 1997), that accounts for 7-8 % of the condensed phase. The addition of O₂ to the OH-naphthalene adduct results in the formation of epoxy-quinone (C₁₀H₆O₃ at *m/z* 175.04), representing 5-8 % of the particle phase. Other important C₁₀ ring retaining compounds are dihydroxy naphthoquinone (C₁₀H₆O₄ at *m/z* 191.04) and 1,4-naphthoquinone (C₁₀H₆O₂ at *m/z* 159.04). This latter has multiple formation routes, either from reaction of OH radical with naphthalene or with naphthol (C₁₀H₈O at *m/z* 145.07), or from the photodegradation of nitronaphthalene (C₁₀H₇NO₂ at *m/z* 174.05) (Atkinson et al., 1989; Kautzman et al., 2010), potentially explaining the low abundance of the latter (< 1 % in mass) alongside with its reaction product with OH, nitro-naphthol (C₁₀H₇NO₃ at *m/z* 190.05). At both high and low NO_x conditions, the NO₂⁺ signal in the particle phase did not exceed 3 % out of the aerosol mass detected by CHARON-PTR-ToF-MS meaning that the nitro-derivates of naphthalene did not undergo strong fragmentation. The observed low yields of nitro-derivates during the photo oxidation of naphthalene is in agreement with previous studies (Kautzman et al., 2010; Lee and Lane, 2009; Sasaki et al., 1997), but we should also consider that the UV lights used, which peaked at 310 nm, may induce photolysis of nitronaphthalene and other nitro-derivates, as previously reported in chamber experiments with similar UV lamps (Healy et al., 2012).

The formation of C₉ and C₇ products can be explained by H-abstraction of 2-formyl cinnamaldehyde, leading to a formyl peroxy radical that subsequently reacts with NO to form an alkoxy radical implying the loss of CO₂ group (Kautzman et al., 2010). The C₉ compounds contribute by 6-9 % to the gas phase and are the second highest contributors to the particle phase with 16-20 % of the total organic mass. Identified chemical formulas include C₉H₆O₂ (at *m/z* 147.05) which can be either benzopyrone (also known as coumarin) or indene-dione, as well as indanone (C₉H₈O at *m/z* 133.06) first detected by Lee and



Lane (2009). No formation mechanism has been proposed for these products so far, but their molecular structure clearly indicates a rearrangement following ring opening, to form either a new ring at 6 atoms including one oxygen in the case of coumarin, or at 5 atoms for the indene-dione and indanone. This ring closure is a common feature in the case of dialdehydes oxidation, as explained by Lannuque and Sartelet (2024), which may support the hypothesis that these compounds originated from 2-formyl cinnamaldehyde. Further photo-oxidation of coumarin may lead to hydroxycoumarin ($C_9H_6O_3$ at m/z 163.04) accounting for 2.2 % of the gas phase and 4-6 % of the particle phase. A more oxygenated compound, dihydroxy-indanedione ($C_9H_6O_4$ at m/z 179.04), was previously identified by Lee et al. (2018). Logically, this compound was mainly present in the condensed phase with 3-4 % of the total SOA mass.

C_8 oxidation products make up a good 18-35 % and 10-11 % of the gas and particle phases, respectively. Phthaldialdehyde and phthalic anhydride largely dominate the C_8 compounds and are of particular importance in the gas phase. Phthaldialdehyde ($C_8H_6O_2$ at m/z 135.05), is both a first- and second-generation ring-opening product of the OH radical reaction with naphthalene, with the second-generation pathway expected to originate from the reaction of OH radical with 2-formyl cinnamaldehyde (Sasaki et al., 1997; Wang et al., 2007). Further addition of OH radical to phthaldialdehyde will lead to hydroxy phthaldehyde / hydroxy phthalide ($C_8H_6O_3$ at m/z 151.04) that makes up 3.7 % of SOA (Table 3), while the H-abstraction followed by intramolecular cyclization results in phthalic anhydride ($C_8H_4O_3$ at m/z 149.03) making up 2-3% of the condensed phase, and 10-14 % in gas phase (Table 3) previously observed by Wang et al. (2007).

C_7 compounds are relatively less abundant accounting for 3 % of the gas phase products and less than 1 % of SOA. They include compounds like benzoic acid ($C_7H_6O_2$ at m/z 123.05) and benzaldehyde (C_7H_6O at m/z 107.05).

Only two C_6 compounds are detected and represent 3-4 % of the total gas products and only 1 % of the SOA yield. The dominant C_6 in the gaseous phase is $C_6H_{10}O_2$ (at m/z 115.07) with 1.3 %, which can be dimethyloxolanone or hexanedione. The former can be formed from the oxidation of phthaldialdehyde, implying the opening of the second aromatic cycle (Kautzman et al., 2010). Another minor C_6 compound is catechol or benzoquinone ($C_6H_4O_2$ at m/z 110.02).

C_5 products account for only 3-6 % of the gaseous phase and less than 2 % of SOA. A major detected compound is $C_5H_8O_2$ at m/z 101.06 (1.6 %) which can be assigned as methyl furan or 4-oxopentanal.

The C_2 - C_4 products are more volatile, all together make less than 2 % of the total SOA mass but present a considerable fraction of the gas phase products with 18 % for C_4 , 26 % for C_3 , and 4 % for C_2 . The major C_4 contributor is $C_4H_8O_2$ (at m/z 89.06) representing 12 % of the gas phase products. It is tentatively assigned to hydroxybutanal or butanoic acid. Almost all the C_3 fraction is represented by propanoic acid ($C_3H_6O_2$ at m/z 75.04) with 12-20 % contribution to the gas phase products, and methylglyoxal ($C_3H_4O_2$ at m/z 73.03) up to 5 %. The C_2 compound is tentatively assigned to the PAN fragment $C_2H_4O_3$ detected at m/z 77.02 (1.4 %) (Müller et al., 2012).

3.3 Experimentally derived and estimated gas-particle phase partitioning

A two-dimensional space, the 2D-VBS framework (Donahue et al., 2011; Murphy et al., 2012), is used to describe the compounds distribution as function of volatility ($\log_{10}C^*$) and the O/C ratio (Fig. 5) or the oxidation state of carbon (OSc) (Fig.



S4). Figures 5a and 5b display the distribution of measured volatilities for the major compounds detected in both gas and particle phases for m-xylene and naphthalene, respectively, under high NO_x conditions. The volatilities of the identified compounds are in the range of IVOCs (light blue) to SVOCs (light green). Data points are indicated for the experiments at 280 K (purple circles) and 295 K (red circles), and the size of the circles is proportional to the mass concentration (in $\text{m}^3 \mu\text{g}^{-1}$) of each ion in the particle phase.

For m-xylene approximately out of 110 ions detected in the particle phase, half of them is exclusively found in the particle phase. This fraction should populate a low volatility area (as ELVOC), and it is not represented in this 2D-VBS (Fig.5a) but represents more than 30 % of the SOA mass. Among the remaining ions that partition between the two phases, only 18 are considered in Fig.5a, either because more important in term of mass or because they are considered parent ions following Gkatzelis et al. (2018) method. About 24 to 58 % of the particle mass populate the SVOCs regime, while 8 to 16 % are in IVOCs regime, depending on the experimental conditions. In a recent work the SOA components from OH radical oxidation of toluene populated mostly the SVOC range and only 10-17 % was exclusively in the particle phase (Lannuque et al., 2023), probably because of higher initial VOC concentration and lower OH exposure (10-20 h compared to 1.3-3 days in this study) leading to a less advanced oxidation. But overall, the effect of temperature observed is quite similar for the two chemical systems. For naphthalene at 280 K, out of the 110 ions detected in the particle phase, 40 ions are exclusively observed in the particle phase, making up 5 % only of the condensed mass fraction. For the selected 20 compounds that partition between the two phases, approximately 78-95 % of their SOA mass populates SVOC regime and 3-17 % lies in the IVOC portion. The larger skeleton structure of naphthalene oxidation products, even first generation, can explain the high fraction of SOA in the SVOC regime (predominantly C_{8-10} compounds).

The derived saturation concentration (C_i^*) values range between 1 to $6919 \mu\text{g m}^{-3}$, comparable to other SOA systems (Gkatzelis et al., 2018; Kostenidou et al., 2024; Lannuque et al., 2023). Previous studies on biogenic VOCs reported a decreasing volatility with increasing OSc (Gkatzelis et al., 2018; Jimenez et al., 2009; Kroll et al., 2011), while the present works and previous investigations on anthropogenic VOCs (toluene and gasoline vehicle emissions) did not confirm such a trend (Kostenidou et al., 2024; Lannuque et al., 2023).

Figures 5c and 5d present $\Delta\log_{10}C_i^*$ (the difference of $\log_{10}C_i^*$ between experiments at 280 and 295 K) values that vary from 0.06 to 1.08 as a function of carbon number and oxygen number (tables S2 and S3). For m-xylene oxidation products (Fig. 5c), $\Delta\log_{10}C_i^*$ decreases with increasing carbon number. Indeed, the $\text{C}_5\text{-C}_8$ products bearing 3 to 5 oxygen atoms (darker green markers) lie at the bottom of the plot generally exhibiting $\Delta\log_{10}C_i^*$ values below 0.4, emphasizing the effect of oxygen atoms in reducing the volatility of these compounds. The C_3 compounds, tentatively associated to methylglyoxal and propanoic acid, exhibit also moderate $\Delta\log_{10}C_i^*$, probably because they are quite volatile at both temperatures (table 2). Only few among the identified $\text{C}_4\text{-C}_5$ products exhibit $\Delta\log_{10}C_i^*$ values above 0.6 and are tentatively identified as ring opening products (aldehydes, acids and furandiones).

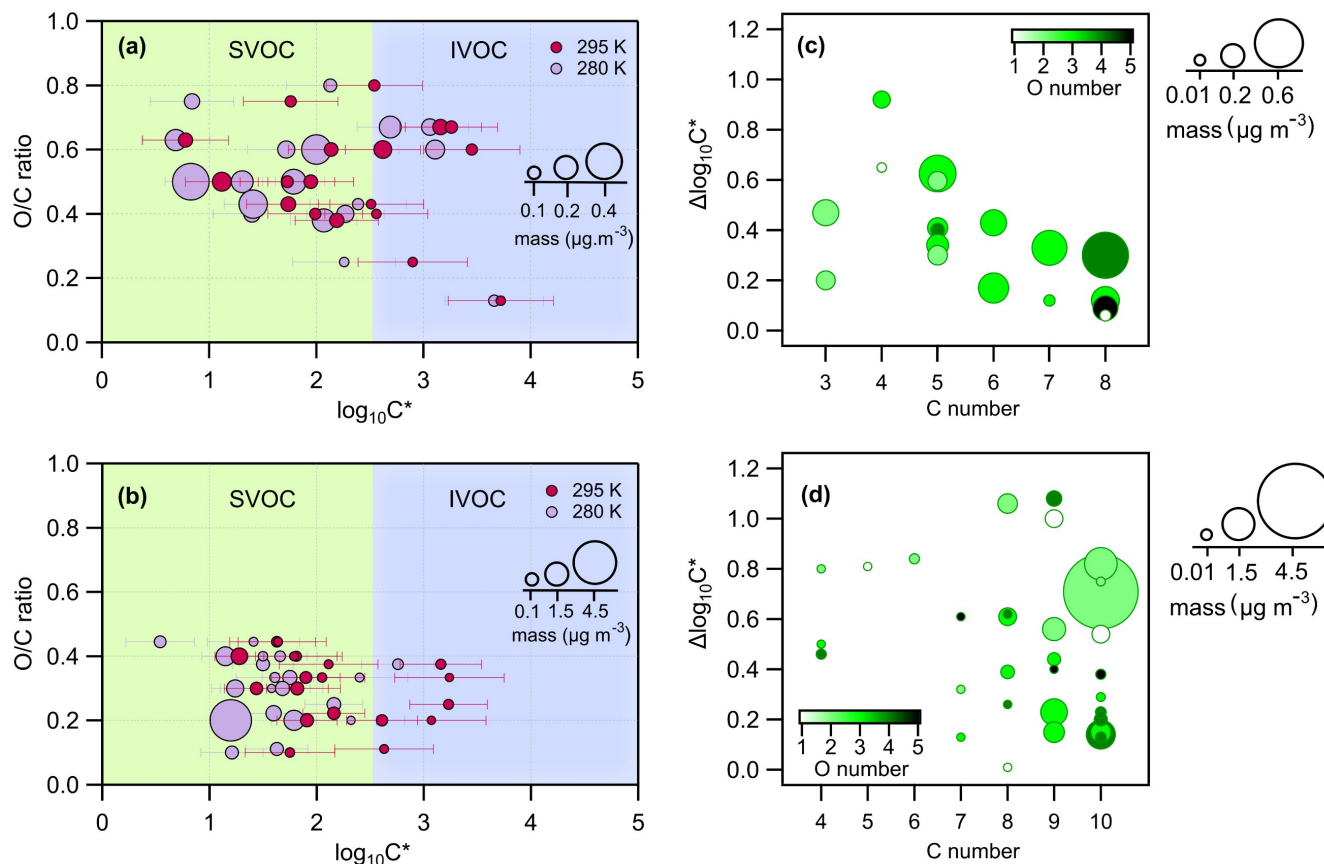


Figure 5. Panels (a) and (b) present the O/C ratio for the detected parent ions of m-xylene and naphthalene photooxidation, respectively, as a function of averaged saturation concentration ($\log_{10} C_i^*$ in $\mu\text{g m}^{-3}$). The size of the circles denotes the mass of each species. Experiment carried out at 280 K is in light violet while the one carried out at 295 K are in magenta. Panels (c) and (d) present $\Delta \log_{10} C_i^*$ as function of carbon number, colour scaled by oxygen number and sized by the mass (in $\mu\text{g m}^{-3}$) of each compound at 280 K for m-xylene and naphthalene oxidation products, respectively.

480

Naphthalene oxidation products on the other hand (Fig. 5d) exhibit a different behaviour. Most of the relevant reaction products are associated to $\text{C}_{8-10}\text{H}_{4-10}\text{O}_{1-4}$ products, accounting for 90% of the SOA mass and have at least one aromatic ring. Those compounds span a broad range of $\Delta \log_{10} C_i^*$ depending on the number of oxygen atoms (from 1 to 5) and the specific functionalities. Compared to m-xylene, the most important naphthalene SOA-products are less oxygenated and seem to be more temperature-sensitive.

485

3.4 Comparison of experimentally derived and calculated volatilities

The experimentally derived volatilities are here compared to the estimated ones from pure-liquid saturation vapour pressure using Volcalc based on SIMPOL.1 (Meredith et al., 2023; Pankow and Asher, 2008; Riemer, 2023). Volatilities from the two methods are presented in Figs. 6a and 6b for both m-xylene and naphthalene oxidation products at 280 K, respectively, and in



490 Fig. S5 for $T = 295$ K. In both cases, there is a considerable discrepancy between the observed and calculated values, the latter ones spanning a larger range of volatilities. For m-xylene SOA, the theoretical approach tends to largely overestimate the volatility of small and oxygenated compounds below m/z 120, similarly to recent investigations using different techniques as SV-TAG coupled to GC-MS, thermal desorption-AMS and FIGAERO-CIMS and CHARON (Stark et al., 2017; Ijaz et al., 2024; Liang et al., 2023).

495 For some light carbonyl compounds present among the m-xylene reaction products, the disagreement can be potentially explained by presence of ammonium ions (NH_4^+) in the seeds that can act as a catalyst for accretion reactions such as aldol condensation (Li et al., 2022, 2011; Nozière et al., 2010; Sareen et al., 2010) as well as acetal and hemiacetal formation (Jang et al., 2002; Li et al., 2022; Loeffler et al., 2006; Shapiro et al., 2009) shifting the equilibrium to the condensed phase for these molecules. Furthermore, Lannuque et al. (2023) have achieved better model representation of experimental SOA mass

500 concentration after including interactions between aldehydes as methylglyoxal and inorganic compounds (such as ammonium). Those reactions are also catalysed in the presence of water, especially for highly oxidized hydrophilic compounds (Meng et al., 2024). For some other compounds, as functionalized acids and some dialdehydes, disagreements may arise from the fragmentation in the mass spectrometer. Despite a relatively low E/N value (68 Td) used in this work, fragmentation may still occur, particularly in polyfunctional products (Leglise et al., 2019). We also tested the fragmentation of several compounds in

505 a separate work (Lannuque et al., 2023) where we could observe low or negligible fragmentation for methylglyoxal, furans, furfurals, maleic acids and anhydrides but important fragmentation for small linear aldehydes.

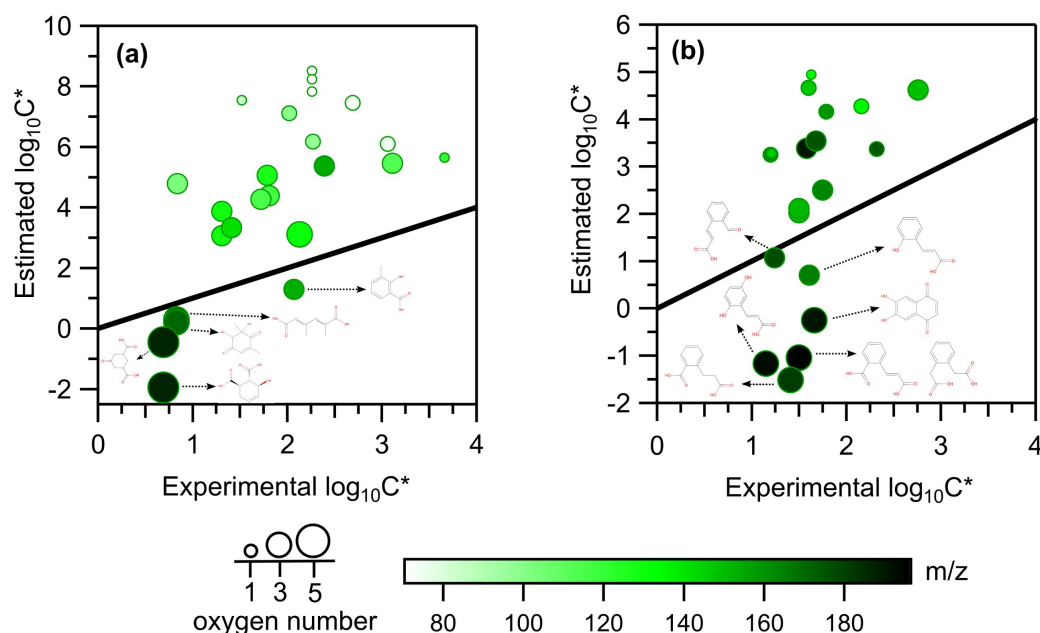


Figure 6. Theoretical (y-axis) versus experimental $\log_{10} C_i^*$ values (x-axis) for (a) m-xylene and (b) naphthalene oxidation products at 280 K. The black line is the 1:1 fit. The size of the markers is proportional to the oxygen number. The colour gradient corresponds to m/z of the detected compounds.



For naphthalene SOA products, larger discrepancies are observed for larger compounds ($m/z \geq 160$) associated to C_{8-10} compounds bearing multiple functional groups. For such type of compounds, the model predicts very low volatilities (O'Meara et al., 2014) also demonstrating that SIMPOL.1 consistently overestimates temperature-induced volatility changes for highly oxygenated compounds (such as hydroxylated ketones and diacids). These discrepancies are attributed to the additive nature of SIMPOL.1's functional group contribution framework. At 280 K, a carboxylic acid group (-COOH) decreases the saturation vapor pressure by nearly a factor of 6000, a hydroxyl group (-OH) by factor 200, while a ketone group (=O) reduces it by less than a factor of 9. It is also worth noting that multiple structural isomers are not distinguished in our work, and this may also introduce some uncertainties. An example is provided by 1,2-naphthoquinone and 1,4-naphthoquinone owing quite different vapour pressure making the former potentially more interesting in the particle phase (McWhinney et al., 2013). Liang et al. (2023) and Dang et al., (2019) also reported very different gas-particle partitioning behaviour and vapour pressures values among isomers. Barley and McFiggans (2010) and Peräkylä et al. (2020) highlighted significant overpredictions for diacids and polyfunctional compounds, attributing these errors to the model's parameterizations and group contributions. This work therefore aligns with previous findings and suggests that vapor pressures of multifunctional compounds of the aerosol are still not well estimated by models.

4 Conclusion

This study presents a detailed experimental investigation of the OH-initiated photooxidation of two anthropogenic aromatic precursors: m-xylene and naphthalene, using an oxidation flow reactor system under different NO_x and temperature conditions. SOA yields are found to strongly depend on the experimental conditions (temperature, VOC/ NO_x ratios), in agreement with previous studies. The CHARON-inlet coupled to a PTR-ToF-MS successfully quantified between 65-80 % of the total organic mass measured from an aerosol mass spectrometer (HR-ToF-AMS). Despite possible fragmentation of the measured compounds, the major products both in the gas and particulate phases are confirmed through intercomparison with the literature. Major gas phase products of m-xylene SOA are C_3 , C_5 and C_8 compounds whereas the particle phase products are dominated by C_6 - C_8 compounds. For naphthalene experiments, gas phase products are dominated by C_8 and C_{10} compounds, while the particle phase composition mainly consists of C_8 , C_9 and C_{10} compounds. Nitro-derivatives (nitrogen containing compounds + PAN fragment) measured in both phases did not exceed 7 % in naphthalene experiments whereas they could reach up to 20 % in the m-xylene experiments.

The volatility properties of the individual compounds are presented in a 2D-VBS framework: 24-58 % of the SOA mass generated by m-xylene populates the SVOC regime and 8-16 % populates the IVOCs regime, while the naphthalene SOA mass is mostly (up to 95 %) found in the SVOC regime. No clear correlation between the volatility values and the increasing oxidation state (OSc) could be observed, in agreement with previous studies on anthropogenic monoaromatic precursors. Temperature variation, from 295 to 280 K, induced an expected decrease in volatility ($D\log_{10}C_i^*$) ranging from 0.06 to 1.08. The magnitude of $\Delta\log_{10}C_i^*$ seems to be controlled by multiple parameters, as temperature, carbon number, oxygen number



and specific chemical moieties. When experimentally derived volatilities are compared to a group contribution parameterization model based on pure liquid vapour pressure (SIMPOL.1) large discrepancies are observed. The current
545 volatility parameterisations should be further validated using larger datasets from various measurement techniques at different environmental conditions as rarely experiments are carried out at low temperature.

This study advances our understanding of SOA composition and gas-particle partitioning at different and relevant atmospheric conditions and also holds some implications for urban air quality management and climate modelling. The observed temperature-dependent shifts in SOA mass loadings and volatility highlight the importance of accounting for seasonal
550 variations, particularly in urban areas with high anthropogenic VOC emissions. Furthermore, the findings underscore the need to refine current air quality and climate models by incorporating more recent findings and real-world atmospheric conditions, paving the way for more accurate predictions of aerosol impacts on air quality, climate, and public health.

Data availability

Finalized data are mostly available in supplementary material. More detailed data are available on request.

555 Supplementary material

Competing interests

The authors declare that they have no conflict of interest.

Author contribution

MS, JK, and BD designed the experimental setup. MS, JK, BTR and BD performed the experiments and data treatment. MS,
560 BD and JK analysed and interpreted the data. MS ran the SIMPOL.1 model. MS drafted the article. All the co-authors revised the article.

Financial Support

This work was funded by the POLEMICS project of the Agence Nationale de la Recherche (ANR) program (grant ANR-18-CE22-0011), and the MAESTRO-EU6 project (ADEME CORTEA n. 1866C0001), the French government under the France
565 2030 investment plan, as part of the Initiative d'Excellence d'Aix-Marseille Université – A*MIDEX ” AMX-21-PEP-016, the French national research agency (ANR-22-CE22-0003-01) and the Environmental Sciences doctoral school (ED 251). BD acknowledges the MITI program from CNRS for the financial support allowing the design and the construction of the new oxidation flow reactor (OFR) deployed in this study.



References

- 570 Ahlberg, E., Eriksson, A., Brune, W. H., Roldin, P., and Svenningsson, B.: Effect of salt seed particle surface area, composition and phase on secondary organic aerosol mass yields in oxidation flow reactors, *Atmos. Chem. Phys.*, 19, 2701–2712, <https://doi.org/10.5194/acp-19-2701-2019>, 2019.
- Anderson, J. O., Thundiyil, J. G., and Stolbach, A.: Clearing the Air: A Review of the Effects of Particulate Matter Air Pollution on Human Health, *J. Med. Toxicol.*, 8, 166–175, <https://doi.org/10.1007/s13181-011-0203-1>, 2012.
- 575 Aoki, N., Inomata, S., and Tanimoto, H.: Detection of C1–C5 alkyl nitrates by proton transfer reaction time-of-flight mass spectrometry, *International Journal of Mass Spectrometry*, 263, 12–21, <https://doi.org/10.1016/j.ijms.2006.11.018>, 2007.
- Atkinson, R., Aschmann, S. M., and Zielinska, B.: GAS-PHASE ATMOSPHERIC CHEMISTRY OF 1- AND 2-NITRONAPHTHALENE AND 1,4-NAPHTHOQUINONE, 1989.
- Atkinson, R., Aschmann, S. M., and Arey, J.: Formation of ring-retaining products from the OH radical-initiated reactions of *o* -, *m* -, and *p* -xylene, *Int J of Chemical Kinetics*, 23, 77–97, <https://doi.org/10.1002/kin.550230108>, 1991.
- 580 Aumont, B., Camredon, M., Mouchel-Vallon, C., La, S., Ouzebidou, F., Valorso, R., Lee-Taylor, J., and Madronich, S.: Modeling the influence of alkane molecular structure on secondary organic aerosol formation, *Faraday Discuss.*, 165, 105, <https://doi.org/10.1039/c3fd00029j>, 2013.
- Barley, M. H. and McFiggans, G.: The critical assessment of vapour pressure estimation methods for use in modelling the formation of atmospheric organic aerosol, *Atmos. Chem. Phys.*, 10, 749–767, <https://doi.org/10.5194/acp-10-749-2010>, 2010.
- 585 Baudic, A., Gros, V., Sauvage, S., Locoge, N., Sanchez, O., Sarda-Estève, R., Kalogridis, C., Petit, J.-E., Bonnaire, N., Baisnée, D., Favez, O., Albinet, A., Sciare, J., and Bonsang, B.: Seasonal variability and source apportionment of volatile organic compounds (VOCs) in the Paris megacity (France), *Atmos. Chem. Phys.*, 16, 11961–11989, <https://doi.org/10.5194/acp-16-11961-2016>, 2016.
- 590 Berlinger, B., Fehérvári, P., Kővágó, C., Lányi, K., Máti, G., Mackei, M., and Könyves, L.: There Is Still a Need for a Comprehensive Investigation of the Health Consequences of Exposure to Urban Air with Special Regard to Particulate Matter (PM) and Cardiovascular Effects, *Atmosphere*, 15, 296, <https://doi.org/10.3390/atmos15030296>, 2024.
- Birdsall, A. W. and Elrod, M. J.: Comprehensive NO-Dependent Study of the Products of the Oxidation of Atmospherically Relevant Aromatic Compounds, *J. Phys. Chem. A*, 115, 5397–5407, <https://doi.org/10.1021/jp2010327>, 2011.
- 595 Bloss, C., Wagner, V., Jenkin, M. E., Volkamer, R., Bloss, W. J., Lee, J. D., Heard, D. E., Wirtz, K., Martin-Reviejo, M., Rea, G., Wenger, J. C., and Pilling, M. J.: Development of a detailed chemical mechanism (MCMv3.1) for the atmospheric oxidation of aromatic hydrocarbons, *Atmos. Chem. Phys.*, 5, 641–664, <https://doi.org/10.5194/acp-5-641-2005>, 2005.
- Bosque, R. and Sales, J.: Polarizabilities of Solvents from the Chemical Composition, *J. Chem. Inf. Comput. Sci.*, 42, 1154–1163, <https://doi.org/10.1021/ci025528x>, 2002.
- 600 Bunce, N. J., Liu, L., Zhu, J., and Lane, D. A.: Reaction of Naphthalene and Its Derivatives with Hydroxyl Radicals in the Gas Phase, *Environ. Sci. Technol.*, 31, 2252–2259, <https://doi.org/10.1021/es960813g>, 1997.
- Calvert, J. G., Atkinson, R., Becker, K. H., Kamens, R. M., Wallington, T. H., Seinfeld, J. H., and Yarwood, G.: *The Mechanisms of Atmospheric Oxidation of Aromatic Hydrocarbons*, Oxford University Press, 2002.



- Calvert, J. G., Orlando, J. J., Stockwell, W. R., and Wallington, T. J.: The Mechanisms of Reactions Influencing Atmospheric
 605 Ozone, Oxford University Press, <https://doi.org/10.1093/oso/9780190233020.001.0001>, 2015.
- Canagaratna, M. R., Jayne, J. T., Jimenez, J. L., Allan, J. D., Alfarra, M. R., Zhang, Q., Onasch, T. B., Drewnick, F., Coe, H.,
 Middlebrook, A., Delia, A., Williams, L. R., Trimborn, A. M., Northway, M. J., DeCarlo, P. F., Kolb, C. E., Davidovits, P.,
 and Worsnop, D. R.: Chemical and microphysical characterization of ambient aerosols with the aerodyne aerosol mass
 spectrometer, *Mass Spectrometry Reviews*, 26, 185–222, <https://doi.org/10.1002/mas.20115>, 2007.
- 610 Cappa, C. D. and Wilson, K. R.: Multi-generation gas-phase oxidation, equilibrium partitioning, and the formation and
 evolution of secondary organic aerosol, *Atmos. Chem. Phys.*, 12, 9505–9528, <https://doi.org/10.5194/acp-12-9505-2012>,
 2012.
- Chan, A. W. H., Kautzman, K. E., Chhabra, P. S., Surratt, J. D., Chan, M. N., Crounse, J. D., Wennberg, P. O., Flagan, R. C.,
 and Seinfeld, J. H.: Secondary organic aerosol formation from photooxidation of naphthalene and alkylnaphthalenes:
 615 implications for oxidation of intermediate volatility organic compounds (IVOCs), *Atmos. Chem. Phys.*, 9, 3049–3060,
<https://doi.org/10.5194/acp-9-3049-2009>, 2009.
- Chen, C.-L., Kacarab, M., Tang, P., and Cocker, D. R.: SOA formation from naphthalene, 1-methylnaphthalene, and 2-
 methylnaphthalene photooxidation, *Atmospheric Environment*, 131, 424–433,
<https://doi.org/10.1016/j.atmosenv.2016.02.007>, 2016.
- 620 Chen, C.-L., Li, L., Tang, P., and Cocker, D. R.: SOA formation from photooxidation of naphthalene and methylnaphthalenes
 with m-xylene and surrogate mixtures, *Atmospheric Environment*, 180, 256–264,
<https://doi.org/10.1016/j.atmosenv.2018.02.051>, 2018.
- Chen, T., Liu, Y., Chu, B., Liu, C., Liu, J., Ge, Y., Ma, Q., Ma, J., and He, H.: Differences of the oxidation process and
 secondary organic aerosol formation at low and high precursor concentrations, *Journal of Environmental Sciences*, 79,
 625 256–263, <https://doi.org/10.1016/j.jes.2018.11.011>, 2019.
- Dang, C., Bannan, T., Shelley, P., Priestley, M., Worrall, S. D., Waters, J., Coe, H., Percival, C. J., and Topping, D.: The effect
 of structure and isomerism on the vapor pressures of organic molecules and its potential atmospheric relevance, *Aerosol
 Science and Technology*, 53, 1040–1055, <https://doi.org/10.1080/02786826.2019.1628177>, 2019.
- DeCarlo, P. F., Kimmel, J. R., Trimborn, A., Northway, M. J., Jayne, J. T., Aiken, A. C., Gonin, M., Fuhrer, K., Horvath, T.,
 630 Docherty, K. S., Worsnop, D. R., and Jimenez, J. L.: Field-Deployable, High-Resolution, Time-of-Flight Aerosol Mass
 Spectrometer, *Analytical Chemistry*, 78, 8281–8289, <https://doi.org/10.1021/ac061249n>, 2006.
- Dodge, M.: Combined use of modeling techniques and smog chamber data to derive ozone-precursor relationships,
 International conference on photochemical oxidant pollution and its control: Proceedings, 881–889, 1977.
- Donahue, N. M., Epstein, S. A., Pandis, S. N., and Robinson, A. L.: A two-dimensional volatility basis set: 1. organic-aerosol
 635 mixing thermodynamics, *Atmos. Chem. Phys.*, 11, 3303–3318, <https://doi.org/10.5194/acp-11-3303-2011>, 2011.
- Duncanu, M., David, M., Kartigeyane, S., Cirtog, M., Doussin, J.-F., and Picquet-Varrault, B.: Measurement of alkyl and
 multifunctional organic nitrates by proton-transfer-reaction mass spectrometry, *Atmos. Meas. Tech.*, 10, 1445–1463,
<https://doi.org/10.5194/amt-10-1445-2017>, 2017.
- Eichler, P., Müller, M., D’Anna, B., and Wisthaler, A.: A novel inlet system for online chemical analysis of semi-volatile
 640 submicron particulate matter, *Atmos. Meas. Tech.*, 8, 1353–1360, <https://doi.org/10.5194/amt-8-1353-2015>, 2015.



European Environment Agency: Europe's air quality status 2021, Publications Office, LU, 2022.

Fan, J. and Zhang, R.: Density Functional Theory Study on OH-Initiated Atmospheric Oxidation of *m*-Xylene, *J. Phys. Chem. A*, 112, 4314–4323, <https://doi.org/10.1021/jp077648j>, 2008.

645 Fang, H., Luo, S., Huang, X., Fu, X., Xiao, S., Zeng, J., Wang, J., Zhang, Y., and Wang, X.: Ambient naphthalene and methylnaphthalenes observed at an urban site in the Pearl River Delta region: Sources and contributions to secondary organic aerosol, *Atmospheric Environment*, 252, 118295, <https://doi.org/10.1016/j.atmosenv.2021.118295>, 2021.

650 Fang, H., Wang, W., Xu, H., Huang, Y., Jiang, H., Wu, T., Li, J., Zha, S., Zhang, J., Zhou, R., and Wang, X.: Sources and secondary transformation potentials of aromatic hydrocarbons observed in a medium-sized city in yangtze river delta region: Emphasis on intermediate-volatility naphthalene, *Atmospheric Environment*, 318, 120239, <https://doi.org/10.1016/j.atmosenv.2023.120239>, 2024.

Forstner, H. J. L., Flagan, R. C., and Seinfeld, J. H.: Secondary Organic Aerosol from the Photooxidation of Aromatic Hydrocarbons: Molecular Composition, *Environ. Sci. Technol.*, 31, 1345–1358, <https://doi.org/10.1021/es9605376>, 1997.

Gioumousis, G. and Stevenson, D. P.: Reactions of Gaseous Molecule Ions with Gaseous Molecules. V. Theory, *The Journal of Chemical Physics*, 29, 294–299, <https://doi.org/10.1063/1.1744477>, 1958.

655 Gkatzelis, G. I., Hohaus, T., Tillmann, R., Gensch, I., Müller, M., Eichler, P., Xu, K.-M., Schlag, P., Schmitt, S. H., Yu, Z., Wegener, R., Kaminski, M., Holzinger, R., Wisthaler, A., and Kiendler-Scharr, A.: Gas-to-particle partitioning of major biogenic oxidation products: a study on freshly formed and aged biogenic SOA, *Atmos. Chem. Phys.*, 18, 12969–12989, <https://doi.org/10.5194/acp-18-12969-2018>, 2018.

660 Heald, C. L., Jacob, D. J., Park, R. J., Russell, L. M., Huebert, B. J., Seinfeld, J. H., Liao, H., and Weber, R. J.: A large organic aerosol source in the free troposphere missing from current models, *Geophysical Research Letters*, 32, 2005GL023831, <https://doi.org/10.1029/2005GL023831>, 2005.

Healy, R. M., Chen, Y., Kourtchev, I., Kalberer, M., O'Shea, D., and Wenger, J. C.: Rapid Formation of Secondary Organic Aerosol from the Photolysis of 1-Nitronaphthalene: Role of Naphthoxy Radical Self-reaction, *Environ. Sci. Technol.*, 46, 11813–11820, <https://doi.org/10.1021/es302841j>, 2012.

665 Henze, D. K., Seinfeld, J. H., Ng, N. L., and Kroll, J. H.: Global modeling of secondary organic aerosol formation from aromatic hydrocarbons: high- vs. low-yield pathways, *Atmos. Chem. Phys.*, 8, 2405–2421, <https://doi.org/10.5194/acp-8-2405-2008>, 2008.

670 Huang, D. D., Kong, L., Gao, J., Lou, S., Qiao, L., Zhou, M., Ma, Y., Zhu, S., Wang, H., Chen, S., Zeng, L., and Huang, C.: Insights into the formation and properties of secondary organic aerosol at a background site in Yangtze River Delta region of China: Aqueous-phase processing vs. photochemical oxidation, *Atmospheric Environment*, 239, 117716, <https://doi.org/10.1016/j.atmosenv.2020.117716>, 2020.

Huang, M., Zhang, W., Hao, L., Wang, Z., Zhao, W., Gu, X., and Fang, L.: Low-Molecular Weight and Oligomeric Components in Secondary Organic Aerosol from the Photooxidation of *p*-Xylene, *J Chinese Chemical Soc*, 55, 456–463, <https://doi.org/10.1002/jccs.200800068>, 2008.

675 Huang, R.-J., Zhang, Y., Bozzetti, C., Ho, K.-F., Cao, J.-J., Han, Y., Daellenbach, K. R., Slowik, J. G., Platt, S. M., Canonaco, F., Zotter, P., Wolf, R., Pieber, S. M., Bruns, E. A., Crippa, M., Ciarelli, G., Piazzalunga, A., Schwikowski, M., Abbaszade, G., Schnelle-Kreis, J., Zimmermann, R., An, Z., Szidat, S., Baltensperger, U., Haddad, I. E., and Prévôt, A. S. H.: High



secondary aerosol contribution to particulate pollution during haze events in China, *Nature*, 514, 218–222, <https://doi.org/10.1038/nature13774>, 2014.

680 Ijaz, A., Temime-Roussel, B., Kammer, J., Mao, J., Simpson, W., Law, K. S., and Barbara, D.: In situ measurements of gas-particle partitioning of organic compounds in Fairbanks, *Faraday Discuss.*, 10.1039.D4FD00175C, <https://doi.org/10.1039/D4FD00175C>, 2024.

Isaacman-VanWertz, G., Massoli, P., O'Brien, R., Lim, C., Franklin, J. P., Moss, J. A., Hunter, J. F., Nowak, J. B., Canagaratna, M. R., Misztal, P. K., Arata, C., Roscioli, J. R., Herndon, S. T., Onasch, T. B., Lambe, A. T., Jayne, J. T., Su, L.,
 685 Knopf, D. A., Goldstein, A. H., Worsnop, D. R., and Kroll, J. H.: Chemical evolution of atmospheric organic carbon over multiple generations of oxidation, *Nature Chem*, 10, 462–468, <https://doi.org/10.1038/s41557-018-0002-2>, 2018.

Jang, M. and Kamens, R. M.: Characterization of Secondary Aerosol from the Photooxidation of Toluene in the Presence of NO_x and 1-Propene, *Environ. Sci. Technol.*, 35, 3626–3639, <https://doi.org/10.1021/es010676+>, 2001.

Jang, M., Czoschke, N. M., Lee, S., and Kamens, R. M.: Heterogeneous Atmospheric Aerosol Production by Acid-Catalyzed
 690 Particle-Phase Reactions, *Science, New Series*, 298, 814–817, <https://doi.org/10.1126/science.1075798>, 2002.

Jenkin, M. E., Saunders, S. M., Wagner, V., and Pilling, M. J.: Protocol for the development of the Master Chemical Mechanism, MCM v3 (Part B): tropospheric degradation of aromatic volatile organic compounds, Part B, 2003.

Jiang, Z., Grosselin, B., Daële, V., Mellouki, A., and Mu, Y.: Seasonal and diurnal variations of BTEX compounds in the semi-urban environment of Orleans, France, *Science of The Total Environment*, 574, 1659–1664,
 695 <https://doi.org/10.1016/j.scitotenv.2016.08.214>, 2017.

Jimenez, J. L., Canagaratna, M. R., Donahue, N. M., Prevot, A. S. H., Zhang, Q., Kroll, J. H., DeCarlo, P. F., Allan, J. D., Coe, H., Ng, N. L., Aiken, A. C., Docherty, K. S., Ulbrich, I. M., Grieshop, A. P., Robinson, A. L., Duplissy, J., Smith, J. D., Wilson, K. R., Lanz, V. A., Hueglin, C., Sun, Y. L., Tian, J., Laaksonen, A., Raatikainen, T., Rautiainen, J., Vaattovaara, P., Ehn, M., Kulmala, M., Tomlinson, J. M., Collins, D. R., Cubison, M. J., E., Dunlea, J., Huffman, J. A., Onasch, T. B., Alfarra, M. R.,
 700 Williams, P. I., Bower, K., Kondo, Y., Schneider, J., Drewnick, F., Borrmann, S., Weimer, S., Demerjian, K., Salcedo, D., Cottrell, L., Griffin, R., Takami, A., Miyoshi, T., Hatakeyama, S., Shimono, A., Sun, J. Y., Zhang, Y. M., Dzepina, K., Kimmel, J. R., Sueper, D., Jayne, J. T., Herndon, S. C., Trimborn, A. M., Williams, L. R., Wood, E. C., Middlebrook, A. M., Kolb, C. E., Baltensperger, U., and Worsnop, D. R.: Evolution of Organic Aerosols in the Atmosphere, *Science*, 326, 1525–1529, <https://doi.org/10.1126/science.1180353>, 2009.

705 Jin, Z.-H., Yu, D., Liu, Y.-X., Tian, Z.-Y., Richter, S., Braun-Unkhoff, M., Naumann, C., and Yang, J.-Z.: An experimental investigation of furfural oxidation and the development of a comprehensive combustion model, *Combustion and Flame*, 226, 200–210, <https://doi.org/10.1016/j.combustflame.2020.12.015>, 2021.

Kamens, R. M., Zhang, H., Chen, E. H., Zhou, Y., Parikh, H. M., Wilson, R. L., Galloway, K. E., and Rosen, E. P.: Secondary organic aerosol formation from toluene in an atmospheric hydrocarbon mixture: Water and particle seed effects, *Atmospheric Environment*, 45, 2324–2334, <https://doi.org/10.1016/j.atmosenv.2010.11.007>, 2011.
 710

Kautzman, K. E., Surratt, J. D., Chan, M. N., Chan, A. W. H., Hersey, S. P., Chhabra, P. S., Dalleska, N. F., Wennberg, P. O., Flagan, R. C., and Seinfeld, J. H.: Chemical Composition of Gas- and Aerosol-Phase Products from the Photooxidation of Naphthalene, *J. Phys. Chem. A*, 114, 913–934, <https://doi.org/10.1021/jp908530s>, 2010.

Kim, D.-Y., Soda, S., Kendo, A., and Oh, J.-H.: Atmospheric Photochemistry in Low-and High-NO_x Regimes, *Journal of Environmental Science International*, 16, 1–8, <https://doi.org/10.5322/JES.2007.16.1.001>, 2007.
 715



Klodt, A. L., Aiona, P. K., MacMillan, A. C., Ji (Julie) Lee, H., Zhang, X., Helgestad, T., Novak, G. A., Lin, P., Laskin, J., Laskin, A., Bertram, T. H., Cappa, C. D., and Nizkorodov, S. A.: Effect of relative humidity, NO_x , and ammonia on the physical properties of naphthalene secondary organic aerosols, *Environ. Sci.: Atmos.*, 3, 991–1007, <https://doi.org/10.1039/D3EA00033H>, 2023.

- 720 Kostenidou, E., Marques, B., Temime-Roussel, B., Liu, Y., Vansevenant, B., Sartelet, K., and D’Anna, B.: Secondary organic aerosol formed by Euro 5 gasoline vehicle emissions: chemical composition and gas-to-particle phase partitioning, *Atmos. Chem. Phys.*, 24, 2705–2729, <https://doi.org/10.5194/acp-24-2705-2024>, 2024.

Kroll, J. H. and Seinfeld, J. H.: Chemistry of secondary organic aerosol: Formation and evolution of low-volatility organics in the atmosphere, *Atmospheric Environment*, 42, 3593–3624, <https://doi.org/10.1016/j.atmosenv.2008.01.003>, 2008.

- 725 Kroll, J. H., Donahue, N. M., Jimenez, J. L., Kessler, S. H., Canagaratna, M. R., Wilson, K. R., Altieri, K. E., Mazzoleni, L. R., Wozniak, A. S., Bluhm, H., Mysak, E. R., Smith, J. D., Kolb, C. E., and Worsnop, D. R.: Carbon oxidation state as a metric for describing the chemistry of atmospheric organic aerosol, *Nature Chem*, 3, 133–139, <https://doi.org/10.1038/nchem.948>, 2011.

- 730 La, Y. S., Camredon, M., Ziemann, P. J., Valorso, R., Matsunaga, A., Lannuque, V., Lee-Taylor, J., Hodzic, A., Madronich, S., and Aumont, B.: Impact of chamber wall loss of gaseous organic compounds on secondary organic aerosol formation: explicit modeling of SOA formation from alkane and alkene oxidation, *Atmos. Chem. Phys.*, 16, 1417–1431, <https://doi.org/10.5194/acp-16-1417-2016>, 2016.

- 735 Lambe, A. T., Chhabra, P. S., Onasch, T. B., Brune, W. H., Hunter, J. F., Kroll, J. H., Cummings, M. J., Brogan, J. F., Parmar, Y., Worsnop, D. R., Kolb, C. E., and Davidovits, P.: Effect of oxidant concentration, exposure time, and seed particles on secondary organic aerosol chemical composition and yield, *Atmos. Chem. Phys.*, 15, 3063–3075, <https://doi.org/10.5194/acp-15-3063-2015>, 2015.

Langevin, P. (1872–1946): Une formule fondamentale de théorie cinétique, *Ann. Chim. et Physique*, 1905, 5, 245, 269–300, 1950.

- 740 Languille, B., Gros, V., Petit, J.-E., Honoré, C., Baudic, A., Perrussel, O., Foret, G., Michoud, V., Truong, F., Bonnaire, N., Sarda-Estève, R., Delmotte, M., Feron, A., Maisonneuve, F., Gaimoz, C., Formenti, P., Kotthaus, S., Haeffelin, M., and Favez, O.: Wood burning: A major source of Volatile Organic Compounds during wintertime in the Paris region, *Science of The Total Environment*, 711, 135055, <https://doi.org/10.1016/j.scitotenv.2019.135055>, 2020.

- 745 Lannuque, V. and Sartelet, K.: Development of a detailed gaseous oxidation scheme of naphthalene for secondary organic aerosol (SOA) formation and speciation, *Atmospheric Chemistry and Physics*, 24, 8589–8606, <https://doi.org/10.5194/acp-24-8589-2024>, 2024.

Lannuque, V., Camredon, M., Couvidat, F., Hodzic, A., Valorso, R., Madronich, S., Bessagnet, B., and Aumont, B.: Exploration of the influence of environmental conditions on secondary organic aerosol formation and organic species properties using explicit simulations: development of the VBS-GECKO parameterization, *Atmos. Chem. Phys.*, 18, 13411–13428, <https://doi.org/10.5194/acp-18-13411-2018>, 2018.

- 750 Lannuque, V., D’Anna, B., Kostenidou, E., Couvidat, F., Martinez-Valiente, A., Eichler, P., Wisthaler, A., Müller, M., Temime-Roussel, B., Valorso, R., and Sartelet, K.: Gas–particle partitioning of toluene oxidation products: an experimental and modeling study, *Atmos. Chem. Phys.*, 23, 15537–15560, <https://doi.org/10.5194/acp-23-15537-2023>, 2023.

Lee, J. Y. and Lane, D. A.: Unique products from the reaction of naphthalene with the hydroxyl radical, *Atmospheric Environment*, 43, 4886–4893, <https://doi.org/10.1016/j.atmosenv.2009.07.018>, 2009.



- 755 Leglise, J., Müller, M., Piel, F., Otto, T., and Wisthaler, A.: Bulk Organic Aerosol Analysis by Proton-Transfer-Reaction Mass Spectrometry: An Improved Methodology for the Determination of Total Organic Mass, O:C and H:C Elemental Ratios, and the Average Molecular Formula, *Anal. Chem.*, 91, 12619–12624, <https://doi.org/10.1021/acs.analchem.9b02949>, 2019.
- Li, K., Wang, W., Ge, M., Li, J., and Wang, D.: Optical properties of secondary organic aerosols generated by photooxidation of aromatic hydrocarbons, *Scientific Reports*, 4, 4922, <https://doi.org/10.1038/srep04922>, 2014.
- 760 Li, K., Li, J., Liggio, J., Wang, W., Ge, M., Liu, Q., Guo, Y., Tong, S., Li, J., Peng, C., Jing, B., Wang, D., and Fu, P.: Enhanced Light Scattering of Secondary Organic Aerosols by Multiphase Reactions, *Environ. Sci. Technol.*, 51, 1285–1292, <https://doi.org/10.1021/acs.est.6b03229>, 2017.
- Li, K., Li, J., Wang, W., Li, J., Peng, C., Wang, D., and Ge, M.: Effects of Gas-Particle Partitioning on Refractive Index and Chemical Composition of *m*-Xylene Secondary Organic Aerosol, *J. Phys. Chem. A*, 122, 3250–3260, 765 <https://doi.org/10.1021/acs.jpca.7b12792>, 2018.
- Li, Y., Zhao, J., Gomez-Hernandez, M., Lavallee, M., Johnson, N. M., and Zhang, R.: Functionality-based formation of secondary organic aerosol from *m*-xylene photooxidation, *Atmos. Chem. Phys.*, 22, 9843–9857, <https://doi.org/10.5194/acp-22-9843-2022>, 2022.
- 770 Li, Z., Schwier, A. N., Sareen, N., and McNeill, V. F.: Reactive processing of formaldehyde and acetaldehyde in aqueous aerosol mimics: surface tension depression and secondary organic products, *Atmos. Chem. Phys.*, 11, 11617–11629, <https://doi.org/10.5194/acp-11-11617-2011>, 2011.
- Liang, Y., Wernis, R. A., Kristensen, K., Kreisberg, N. M., Croteau, P. L., Herndon, S. C., Chan, A. W. H., Ng, N. L., and Goldstein, A. H.: Gas-particle partitioning of semivolatile organic compounds when wildfire smoke comes to town, *Atmos. Chem. Phys.*, 23, 12441–12454, <https://doi.org/10.5194/acp-23-12441-2023>, 2023.
- 775 Liu, J., Zhu, S., Guo, T., Jia, B., Xu, L., Chen, J., and Cheng, P.: Smog chamber study of secondary organic aerosol formation from gas- and particle-phase naphthalene ozonolysis, *Atmospheric Environment*, 294, 119490, <https://doi.org/10.1016/j.atmosenv.2022.119490>, 2023.
- Liu, K., Hua, S., and Song, L.: PM_{2.5} Exposure and Asthma Development: The Key Role of Oxidative Stress, *Oxidative Medicine and Cellular Longevity*, 2022, 1–12, <https://doi.org/10.1155/2022/3618806>, 2022a.
- 780 Liu, M. and Matsui, H.: Impacts of Climate Change on Particulate Matter (PM), in: *Handbook of Air Quality and Climate Change*, edited by: Akimoto, H. and Tanimoto, H., Springer Nature Singapore, Singapore, 1–18, https://doi.org/10.1007/978-981-15-2527-8_39-1, 2020.
- Liu, M., Bi, J., and Ma, Z.: Visibility-Based PM_{2.5} Concentrations in China: 1957–1964 and 1973–2014, *Environ. Sci. Technol.*, 51, 13161–13169, <https://doi.org/10.1021/acs.est.7b03468>, 2017.
- 785 Liu, S., Wang, Y., Xu, X., and Wang, G.: Effects of NO₂ and RH on secondary organic aerosol formation and light absorption from OH oxidation of *o*-xylene, *Chemosphere*, 308, 136541, <https://doi.org/10.1016/j.chemosphere.2022.136541>, 2022b.
- Liu, X., Day, D. A., Krechmer, J. E., Ziemann, P. J., and Jimenez, J. L.: Determining Activity Coefficients of SOA from Isothermal Evaporation in a Laboratory Chamber, *Environ. Sci. Technol. Lett.*, 8, 212–217, <https://doi.org/10.1021/acs.estlett.0c00888>, 2021.
- 790 Loeffler, K. W., Koehler, C. A., Paul, N. M., and De Haan, D. O.: Oligomer Formation in Evaporating Aqueous Glyoxal and Methyl Glyoxal Solutions, *Environ. Sci. Technol.*, 40, 6318–6323, <https://doi.org/10.1021/es060810w>, 2006.



- Loza, C. L., Chhabra, P. S., Yee, L. D., Craven, J. S., Flagan, R. C., and Seinfeld, J. H.: Chemical aging of <i>p</i>-xylene secondary organic aerosol: laboratory chamber study, *Atmos. Chem. Phys.*, 12, 151–167, <https://doi.org/10.5194/acp-12-151-2012>, 2012.
- 795 Lu, H., Huang, Q., Li, J., Ying, Q., Wang, H., Guo, S., Qin, M., and Hu, J.: Simulation of Regional Secondary Organic Aerosol Formation From Monocyclic Aromatic Hydrocarbons Using a Near-Explicit Chemical Mechanism Constrained by Chamber Experiments, *JGR Atmospheres*, 129, e2023JD040690, <https://doi.org/10.1029/2023JD040690>, 2024.
- Mao, J., Ren, X., Brune, W. H., Olson, J. R., Crawford, J. H., Fried, A., Huey, L. G., Cohen, R. C., Heikes, B., Singh, H. B., Blake, D. R., Sachse, G. W., Diskin, G. S., Hall, S. R., and Shetter, R. E.: Airborne measurement of OH reactivity during
 800 INTEx-B, *Atmos. Chem. Phys.*, 9, 163–173, <https://doi.org/10.5194/acp-9-163-2009>, 2009.
- McWhinney, R. D., Zhou, S., and Abbatt, J. P. D.: Naphthalene SOA: redox activity and naphthoquinone gas–particle partitioning, *Atmos. Chem. Phys.*, 13, 9731–9744, <https://doi.org/10.5194/acp-13-9731-2013>, 2013.
- Meng, X., Wu, Z., Chen, J., Qiu, Y., Zong, T., Song, M., Lee, J., and Hu, M.: Particle phase state and aerosol liquid water greatly impact secondary aerosol formation: insights into phase transition and its role in haze events, *Atmos. Chem. Phys.*, 24, 2399–2414, <https://doi.org/10.5194/acp-24-2399-2024>, 2024.
 805
- Meredith, L. K., Ledford, S. M., Riemer, K., Geffre, P., Graves, K., Honeker, L. K., LeBauer, D., Tfaily, M. M., and Krechmer, J.: Automating methods for estimating metabolite volatility, *Front. Microbiol.*, 14, 1267234, <https://doi.org/10.3389/fmicb.2023.1267234>, 2023.
- Molina, M. J., Zhang, R., Broekhuizen, K., Lei, W., Navarro, R., and Molina, L. T.: Experimental Study of Intermediates from
 810 OH-Initiated Reactions of Toluene, *J. Am. Chem. Soc.*, 121, 10225–10226, <https://doi.org/10.1021/ja992461u>, 1999.
- Montero-Montoya, R., López-Vargas, R., and Arellano-Aguilar, O.: Volatile Organic Compounds in Air: Sources, Distribution, Exposure and Associated Illnesses in Children, *Annals of Global Health*, 84, 225–238, <https://doi.org/10.29024/aogh.910>, 2018.
- Müller, M., Graus, M., Wisthaler, A., Hansel, A., Metzger, A., Dommen, J., and Baltensperger, U.: Analysis of high mass resolution PTR-TOF mass spectra from 1,3,5-trimethylbenzene (TMB) environmental chamber experiments, *Atmos. Chem. Phys.*, 12, 829–843, <https://doi.org/10.5194/acp-12-829-2012>, 2012.
 815
- Müller, M., Mikoviny, T., Jud, W., D’Anna, B., and Wisthaler, A.: A new software tool for the analysis of high resolution PTR-TOF mass spectra, *Chemometrics and Intelligent Laboratory Systems*, 127, 158–165, <https://doi.org/10.1016/j.chemolab.2013.06.011>, 2013.
- 820 Müller, M., Eichler, P., D’Anna, B., Tan, W., and Wisthaler, A.: Direct Sampling and Analysis of Atmospheric Particulate Organic Matter by Proton-Transfer-Reaction Mass Spectrometry, *Anal. Chem.*, 89, 10889–10897, <https://doi.org/10.1021/acs.analchem.7b02582>, 2017.
- Muller, M., Eicher, P., D’Anna, B., Tan, W., and Wisthaler, A.: Direct Sampling and Analysis of Atmospheric Particulate Organic Matter by Proton-Transfer-Reaction Mass Spectrometry, *Analytical Chemistry*, 89, 10889–10897,
 825 <https://doi.org/10.1021/acs.analchem.7b02582>, 2017.
- Murphy, B. N., Donahue, N. M., Fountoukis, C., Dall’Osto, M., O’Dowd, C., Kiendler-Scharr, A., and Pandis, S. N.: Functionalization and fragmentation during ambient organic aerosol aging: application of the 2-D volatility basis set to field studies, *Atmos. Chem. Phys.*, 12, 10797–10816, <https://doi.org/10.5194/acp-12-10797-2012>, 2012.



- 830 NARSTO. and Electric Power Research Institute.: An assessment of tropospheric ozone pollution : a North American perspective, EPRI, 2000.
- Ng, N. L., Kroll, J. H., Chan, A. W. H., Chhabra, P. S., Flagan, R. C., and Seinfeld, J. H.: Secondary organic aerosol formation from *m*-xylene, toluene, and benzene, *Atmos. Chem. Phys.*, 7, 3909–3922, <https://doi.org/10.5194/acp-7-3909-2007>, 2007.
- 835 Nie, W., Yan, C., Huang, D., Wang, Z., Liu, Y., Qiao, X., Guo, Y., Tian, L., Zheng, P., Xu, Z., Li, Y., Xu, Z., Qi, X., Sun, P., Wang, J., Zheng, F., Li, X., Yin, R., Dallenbach, K., Bianchi, F., Petäjä, T., Zhang, Y., Wang, M., Schervish, M., Wang, S., Qiao, L., Wang, Q., Zhou, M., Wang, H., Yu, C., Yao, D., Guo, H., Ye, P., Lee, S., Li, Y., Liu, Y., Chi, X., Kerminen, V., Ehn, M., Donahue, N., Wang, T., Huang, C., Kulmala, M., Worsnop, D., Jiang, J., and Ding, A.: Secondary organic aerosol formed by condensing anthropogenic vapours over China's megacities, *NATURE GEOSCIENCE*, 15, 255–+, <https://doi.org/10.1038/s41561-022-00922-5>, 2022.
- 840 Nishino, N., Arey, J., and Atkinson, R.: Formation and Reactions of 2-Formylcinnamaldehyde in the OH Radical-Initiated Reaction of Naphthalene, *Environ. Sci. Technol.*, 43, 1349–1353, <https://doi.org/10.1021/es802477s>, 2009.
- Nozière, B., Dziedzic, P., and Córdoba, A.: Inorganic ammonium salts and carbonate salts are efficient catalysts for aldol condensation in atmospheric aerosols, *Phys. Chem. Chem. Phys.*, 12, 3864, <https://doi.org/10.1039/b924443c>, 2010.
- Odum, J. R., Hoffmann, T., Bowman, F., Collins, D., Flagan, R. C., and Seinfeld, J. H.: Gas/Particle Partitioning and Secondary Organic Aerosol Yields, *Environ. Sci. Technol.*, 30, 2580–2585, <https://doi.org/10.1021/es950943+>, 1996.
- 845 Odum, J. R., Jungkamp, T. P. W., Griffin, R. J., Forstner, H. J. L., Flagan, R. C., and Seinfeld, J. H.: Aromatics, Reformulated Gasoline, and Atmospheric Organic Aerosol Formation, *Environ. Sci. Technol.*, 31, 1890–1897, <https://doi.org/10.1021/es960535l>, 1997.
- O'Meara, S., Booth, A. M., Barley, M. H., Topping, D., and McFiggans, G.: An assessment of vapour pressure estimation methods, *Phys. Chem. Chem. Phys.*, 16, 19453–19469, <https://doi.org/10.1039/C4CP00857J>, 2014.
- 850 Pan, S. and Wang, L.: Atmospheric Oxidation Mechanism of *m*-Xylene Initiated by OH Radical, *J. Phys. Chem. A*, 118, 10778–10787, <https://doi.org/10.1021/jp506815v>, 2014.
- Pang, X.: Biogenic volatile organic compound analyses by PTR-TOF-MS: Calibration, humidity effect and reduced electric field dependency, *Journal of Environmental Sciences*, 32, 196–206, <https://doi.org/10.1016/j.jes.2015.01.013>, 2015.
- 855 Pankow, J. F. and Asher, W. E.: SIMPOL.1: a simple group contribution method for predicting vapor pressures and enthalpies of vaporization of multifunctional organic compounds, *Atmos. Chem. Phys.*, 8, 2773–2796, <https://doi.org/10.5194/acp-8-2773-2008>, 2008.
- Peng, Y., Wang, H., Gao, Y., Jing, S., Zhu, S., Huang, D., Hao, P., Lou, S., Cheng, T., Huang, C., and Zhang, X.: Real-time measurement of phase partitioning of organic compounds using a proton-transfer-reaction time-of-flight mass spectrometer coupled to a CHARON inlet, *ATMOSPHERIC MEASUREMENT TECHNIQUES*, 16, 15–28, <https://doi.org/10.5194/amt-16-15-2023>, 2023.
- 860 Peräkylä, O., Riva, M., Heikkinen, L., Quéléver, L., Roldin, P., and Ehn, M.: Experimental investigation into the volatilities of highly oxygenated organic molecules (HOMs), *Atmos. Chem. Phys.*, 20, 649–669, <https://doi.org/10.5194/acp-20-649-2020>, 2020.



- 865 Piel, F., Müller, M., Winkler, K., Skytte af Sætra, J., and Wisthaler, A.: Introducing the extended volatility range proton-transfer-reaction mass spectrometer (EVR PTR-MS), *Atmos. Meas. Tech.*, 14, 1355–1363, <https://doi.org/10.5194/amt-14-1355-2021>, 2021.
- Qi, L., Nakao, S., Tang, P., and Iii, D. R. C.: Temperature effect on physical and chemical properties of secondary organic aerosol from m-xylene photooxidation, *Atmos. Chem. Phys.*, <https://doi.org/10.5194/acp-10-3847-2010>, 2010.
- 870 Qi, X., Zhu, S., Zhu, C., Hu, J., Lou, S., Xu, L., Dong, J., and Cheng, P.: Smog chamber study of the effects of NO_x and NH₃ on the formation of secondary organic aerosols and optical properties from photo-oxidation of toluene, *Science of The Total Environment*, 727, 138632, <https://doi.org/10.1016/j.scitotenv.2020.138632>, 2020.
- Qu, X., Zhang, Q., and Wang, W.: Mechanism for OH-initiated photooxidation of naphthalene in the presence of O₂ and NO_x: A DFT study, *Chemical Physics Letters*, 429, 77–85, <https://doi.org/10.1016/j.cplett.2006.08.036>, 2006.
- Riemer, K.: volcalc: Calculate Volatility of Chemical Compounds, Zenodo, <https://doi.org/10.5281/ZENODO.8015155>, 2023.
- 875 Riva, M.: Caractérisation d’une nouvelle voie de formation d’aérosols organiques secondaires (AOS) dans l’atmosphère: Rôle des précurseurs polyaromatiques, Université Bordeaux 1, 2013.
- Salvador, C. M., Chou, C. C.-K., Cheung, H.-C., Ho, T.-T., Tsai, C.-Y., Tsao, T.-M., Tsai, M.-J., and Su, T.-C.: Measurements of submicron organonitrate particles: Implications for the impacts of NO_x pollution in a subtropical forest, *Atmospheric Research*, 245, 105080, <https://doi.org/10.1016/j.atmosres.2020.105080>, 2020.
- 880 Sareen, N., Schwier, A. N., Shapiro, E. L., Mitroo, D., and McNeill, V. F.: Secondary organic material formed by methylglyoxal in aqueous aerosol mimics, *Atmos. Chem. Phys.*, 10, 997–1016, <https://doi.org/10.5194/acp-10-997-2010>, 2010.
- Sasaki, J., Aschmann, S. M., Kwok, E. S. C., Atkinson, R., and Arey, J.: Products of the Gas-Phase OH and NO₃ Radical-Initiated Reactions of Naphthalene, *Environ. Sci. Technol.*, 31, 3173–3179, <https://doi.org/10.1021/es9701523>, 1997.
- 885 Sato, K., Hatakeyama, S., and Imamura, T.: Secondary Organic Aerosol Formation during the Photooxidation of Toluene: NO_x Dependence of Chemical Composition, *J. Phys. Chem. A*, 111, 9796–9808, <https://doi.org/10.1021/jp071419f>, 2007.
- Seinfeld, J. H. and Pandis, S. N.: *Atmospheric chemistry and physics : from air pollution to climate change*, Third edition., John Wiley & Sons, Inc. Hoboken, New Jersey, Hoboken, New Jersey, 2016.
- 890 Sekimoto, K., Li, S.-M., Yuan, B., Koss, A., Coggon, M., Warneke, C., and De Gouw, J.: Calculation of the sensitivity of proton-transfer-reaction mass spectrometry (PTR-MS) for organic trace gases using molecular properties, *International Journal of Mass Spectrometry*, 421, 71–94, <https://doi.org/10.1016/j.ijms.2017.04.006>, 2017.
- Shapiro, E. L., Szprengiel, J., Sareen, N., Jen, C. N., Giordano, M. R., and McNeill, V. F.: Light-absorbing secondary organic material formed by glyoxal in aqueous aerosol mimics, *Atmos. Chem. Phys.*, 9, 2289–2300, <https://doi.org/10.5194/acp-9-2289-2009>, 2009.
- 895 Shrivastava, M., Cappa, C. D., Fan, J., Goldstein, A. H., Guenther, A. B., Jimenez, J. L., Kuang, C., Laskin, A., Martin, S. T., Ng, N. L., Petaja, T., Pierce, J. R., Rasch, P. J., Roldin, P., Seinfeld, J. H., Shilling, J., Smith, J. N., Thornton, J. A., Volkamer, R., Wang, J., Worsnop, D. R., Zaveri, R. A., Zelenyuk, A., and Zhang, Q.: Recent advances in understanding secondary organic aerosol: Implications for global climate forcing, *Reviews of Geophysics*, 55, 509–559, <https://doi.org/10.1002/2016RG000540>, 2017.



- 900 Singh, K. and Tripathi, D.: Particulate Matter and Human Health, in: Environmental Health, edited by: Otsuki, T., IntechOpen, <https://doi.org/10.5772/intechopen.100550>, 2021.
- Song, C., Na, K., and Cocker, D. R.: Impact of the Hydrocarbon to NO_x Ratio on Secondary Organic Aerosol Formation, Environ. Sci. Technol., 39, 3143–3149, <https://doi.org/10.1021/es0493244>, 2005.
- 905 Song, C., Na, K., Warren, B., Malloy, Q., and Cocker, D. R.: Secondary Organic Aerosol Formation from *m*-Xylene in the Absence of NO_x, Environ. Sci. Technol., 41, 7409–7416, <https://doi.org/10.1021/es070429r>, 2007.
- Song, C., He, J., Wu, L., Jin, T., Chen, X., Li, R., Ren, P., Zhang, L., and Mao, H.: Health burden attributable to ambient PM_{2.5} in China, Environmental Pollution, 223, 575–586, <https://doi.org/10.1016/j.envpol.2017.01.060>, 2017.
- Srivastava, D., Vu, T. V., Tong, S., Shi, Z., and Harrison, R. M.: Formation of secondary organic aerosols from anthropogenic precursors in laboratory studies, npj Clim Atmos Sci, 5, 22, <https://doi.org/10.1038/s41612-022-00238-6>, 2022.
- 910 Srivastava, D., Li, W., Tong, S., Shi, Z., and Harrison, R. M.: Characterization of products formed from the oxidation of toluene and *m*-xylene with varying NO_x and OH exposure, Chemosphere, 334, 139002, <https://doi.org/10.1016/j.chemosphere.2023.139002>, 2023.
- 915 Stark, H., Yatavelli, R. L. N., Thompson, S. L., Kang, H., Krechmer, J. E., Kimmel, J. R., Palm, B. B., Hu, W., Hayes, P. L., Day, D. A., Campuzano-Jost, P., Canagaratna, M. R., Jayne, J. T., Worsnop, D. R., and Jimenez, J. L.: Impact of Thermal Decomposition on Thermal Desorption Instruments: Advantage of Thermogram Analysis for Quantifying Volatility Distributions of Organic Species, Environ. Sci. Technol., 51, 8491–8500, <https://doi.org/10.1021/acs.est.7b00160>, 2017.
- Su, T. and Chesnavich, W. J.: Parametrization of the ion–polar molecule collision rate constant by trajectory calculations, The Journal of Chemical Physics, 76, 5183–5185, <https://doi.org/10.1063/1.442828>, 1982.
- 920 Takekawa, H., Minoura, H., and Yamazaki, S.: Temperature dependence of secondary organic aerosol formation by photo-oxidation of hydrocarbons, Atmospheric Environment, 37, 3413–3424, [https://doi.org/10.1016/S1352-2310\(03\)00359-5](https://doi.org/10.1016/S1352-2310(03)00359-5), 2003.
- Tani, A., Hayward, S., and Hewitt, C. N.: Measurement of monoterpenes and related compounds by proton transfer reaction-mass spectrometry (PTR-MS), International Journal of Mass Spectrometry, 223–224, 561–578, [https://doi.org/10.1016/S1387-3806\(02\)00880-1](https://doi.org/10.1016/S1387-3806(02)00880-1), 2003.
- 925 Thangavel, P., Park, D., and Lee, Y.-C.: Recent Insights into Particulate Matter (PM_{2.5})-Mediated Toxicity in Humans: An Overview, IJERPH, 19, 7511, <https://doi.org/10.3390/ijerph19127511>, 2022.
- Tian, L., Huang, D. D., Wang, Q., Zhu, S., Wang, Q., Yan, C., Nie, W., Wang, Z., Qiao, L., Liu, Y., Qiao, X., Guo, Y., Zheng, P., Jing, S., Lou, S., Wang, H., Yu, J. Z., Huang, C., and Li, Y. J.: Underestimated Contribution of Heavy Aromatics to Secondary Organic Aerosol Revealed by Comparative Assessments Using New and Traditional Methods, ACS Earth Space Chem., 7, 110–119, <https://doi.org/10.1021/acsearthspacechem.2c00252>, 2023.
- 930 Tomaz, S.: Etude des composés polyaromatiques dans l’atmosphère: caractérisation moléculaire et processus réactionnels en lien avec l’aérosol organique, Université de Lille, 2015.
- Volkamer, R., Jimenez, J. L., San Martini, F., Dzepina, K., Zhang, Q., Salcedo, D., Molina, L. T., Worsnop, D. R., and Molina, M. J.: Secondary organic aerosol formation from anthropogenic air pollution: Rapid and higher than expected, Geophysical Research Letters, 33, 2006GL026899, <https://doi.org/10.1029/2006GL026899>, 2006.
- 935



- Wang, L., Atkinson, R., and Arey, J.: Dicarbonyl Products of the OH Radical-Initiated Reactions of Naphthalene and the C₁- and C₂-Alkyl naphthalenes, *Environ. Sci. Technol.*, 41, 2803–2810, <https://doi.org/10.1021/es0628102>, 2007.
- Warren, B., Austin, R. L., and Cocker, D. R.: Temperature dependence of secondary organic aerosol, *Atmospheric Environment*, 43, 3548–3555, <https://doi.org/10.1016/j.atmosenv.2009.04.011>, 2009.
- 940 Wu, K., Duan, M., Zhou, J., Zhou, Z., Tan, Q., Song, D., Lu, C., and Deng, Y.: Sources Profiles of Anthropogenic Volatile Organic Compounds from Typical Solvent Used in Chengdu, China, *J. Environ. Eng.*, 146, 05020006, [https://doi.org/10.1061/\(ASCE\)EE.1943-7870.0001739](https://doi.org/10.1061/(ASCE)EE.1943-7870.0001739), 2020.
- Xu, J., Griffin, R. J., Liu, Y., Nakao, S., and Cocker, D. R.: Simulated impact of NO_x on SOA formation from oxidation of toluene and m-xylene, *Atmospheric Environment*, 101, 217–225, <https://doi.org/10.1016/j.atmosenv.2014.11.008>, 2015.
- 945 Xuan, L., Ma, Y., Xing, Y., Meng, Q., Song, J., Chen, T., Wang, H., Wang, P., Zhang, Y., and Gao, P.: Source, temporal variation and health risk of volatile organic compounds (VOCs) from urban traffic in harbin, China, *Environmental Pollution*, 270, 116074, <https://doi.org/10.1016/j.envpol.2020.116074>, 2021.
- Yamasaki, Hiroyasu., Kuwata, Kazuhiro., and Miyamoto, Hiroko.: Effects of ambient temperature on aspects of airborne polycyclic aromatic hydrocarbons, *Environ. Sci. Technol.*, 16, 189–194, <https://doi.org/10.1021/es00098a003>, 1982.
- 950 Zhang, J., Choi, M., Ji, Y., Zhang, R., Zhang, R., and Ying, Q.: Assessing the Uncertainties in Ozone and SOA Predictions due to Different Branching Ratios of the Cresol Pathway in the Toluene-OH Oxidation Mechanism, *ACS Earth Space Chem.*, 5, 1958–1970, <https://doi.org/10.1021/acsearthspacechem.1c00092>, 2021.
- Zhang, P., Huang, J., Shu, J., and Yang, B.: Comparison of secondary organic aerosol (SOA) formation during o-, m-, and p-xylene photooxidation, *Environmental Pollution*, 245, 20–28, <https://doi.org/10.1016/j.envpol.2018.10.118>, 2019a.
- 955 Zhang, Q., Xu, Y., and Jia, L.: Secondary organic aerosol formation from OH-initiated oxidation of <i>m</i>-xylene: effects of relative humidity on yield and chemical composition, *Atmos. Chem. Phys.*, 19, 15007–15021, <https://doi.org/10.5194/acp-19-15007-2019>, 2019b.
- Zhao, J., Zhang, R., Misawa, K., and Shibuya, K.: Experimental product study of the OH-initiated oxidation of m-xylene, *Journal of Photochemistry and Photobiology A: Chemistry*, 176, 199–207, <https://doi.org/10.1016/j.jphotochem.2005.07.013>, 2005.
- 960 Zhu, M., Huang, M., Xue, B., Cai, S., Hu, C., Zhao, W., Gu, X., and Zhang, W.: Chemical analysis of nitro-aromatic compounds of secondary organic aerosol formed from photooxidation of p-xylene with NO_x, *J Chinese Chemical Soc*, 68, 1697–1708, <https://doi.org/10.1002/jccs.202100105>, 2021.